




# Mitochondria transplantation transiently rescues cerebellar neurodegeneration improving mitochondrial function and reducing mitophagy in mice

Received: 20 June 2024

Accepted: 13 March 2025

Published online: 22 March 2025



Shu-Jiao Li<sup>1,6</sup>, Qian-Wen Zheng<sup>2,6</sup>, Jie Zheng<sup>1,6</sup>, Jin-Bao Zhang<sup>3,6</sup>, Hui Liu<sup>1</sup>, Jing-Jing Tie<sup>1</sup>, Kun-Long Zhang<sup>1,4</sup>, Fei-Fei Wu<sup>1</sup>, Xiao-Dong Li<sup>2</sup>, Shuai Zhang<sup>1</sup>, Xin Sun<sup>3</sup> , Yan-Ling Yang<sup>2</sup>  & Ya-Yun Wang<sup>1,5</sup> 

Cerebellar ataxia is the primary manifestation of cerebellar degenerative diseases, and mitochondrial dysfunction in Purkinje cells (PCs) plays a critical role in disease progression. In this study, we investigated the feasibility of mitochondria transplantation as a potential therapeutic approach to rescue cerebellar neurodegeneration and elucidate the associated mechanisms. We constructed a conditional Drp1 knockout model in PCs (PCKO mice), characterized by progressive ataxia. Drp1 knockout resulted in pervasive and progressive apoptosis of PCs and significant activation of surrounding glial cells. Mitochondrial dysfunction, which triggers mitophagy, is a key pathogenic factor contributing to morphological and functional damage in PCs. Transplanting liver-derived mitochondria into the cerebellum of 1-month-old PCKO mice improved mitochondrial function, reduced mitophagy, delayed apoptosis of PCs, and alleviated cerebellar ataxia for up to 3 weeks. These findings demonstrate that mitochondria transplantation holds promise as a therapeutic approach for cerebellar degenerative diseases.

Neurodegenerative diseases (ND) are characterized by the progressive impairment and loss of neuronal function. Cerebellar neurodegenerative diseases (CBND) manifest as cerebellar ataxia including ataxia telangiectasia<sup>1</sup> and spinocerebellar ataxia<sup>2</sup> etc. There was no existing treatment that could completely correct the underlying neurodegenerative disease process<sup>3</sup>.

Mitochondrial dysfunction is a critical factor contributing to ND<sup>4,5</sup>, evidenced by mutations in mitochondria-related genes<sup>6,7</sup>. Notably,

mitochondrial impairment in Purkinje cells (PCs) has been identified as a central mechanism underlying CBND<sup>8–10</sup>. Mitochondrial-targeted interventions in PCs might be a promising therapeutic strategy for combatting CBND<sup>11–13</sup>.

Mitochondria transplantation, a therapeutic approach developed by McCully and colleagues, involves the injection of healthy mitochondria harvested from unaffected tissues into an ischemic organ within the same subject<sup>14</sup>. This technique has been applied to pediatric

<sup>1</sup>Specific Lab for Mitochondrial Plasticity Underlying Nervous System Diseases, National Teaching Demonstration Center, School of Basic Medicine, Air Force Medical University (Fourth Military Medical University), Xi'an, China. <sup>2</sup>Department of Hepatobiliary Surgery, Xi-Jing Hospital, Air Force Medical University (Fourth Military Medical University), Xi'an, China. <sup>3</sup>Department of Pediatrics, Xi-Jing Hospital, Air Force Medical University (Fourth Military Medical University), Xi'an, China. <sup>4</sup>Department of Rehabilitation Medicine, Xi-Jing Hospital, Air Force Medical University (Fourth Military Medical University), Xi'an, China. <sup>5</sup>State Key Laboratory of Military Stomatology, School of Stomatology, Air Force Medical University (Fourth Military Medical University), Xi'an, China. <sup>6</sup>These authors contributed equally: Shu-Jiao Li, Qian-Wen Zheng, Jie Zheng, Jin-Bao Zhang. ✉ e-mail: [sunxin6@fmmu.edu.cn](mailto:sunxin6@fmmu.edu.cn); [yangyanl@fmmu.edu.cn](mailto:yangyanl@fmmu.edu.cn); [wangyy@fmmu.edu.cn](mailto:wangyy@fmmu.edu.cn)

patients with myocardial ischemia, garnering widespread media attention<sup>15</sup>. In the central nervous system, an increasing number of evidence from animal models or cultured cell lines supports the effectiveness of the mitochondria transplantation. Studies have demonstrated that this approach enhances electron transport chain activity in recipient cells, thereby reducing reactive oxygen species (ROS) levels and consequently inhibiting neuronal apoptosis and necrosis<sup>16–18</sup>. Moreover, mitochondria transplantation improves recipient cell function by eliminating damaged mitochondria<sup>19</sup>. Notably, transplanting healthy mitochondria has been shown to enhance neurological function and improve motor ability in transgenic mice with Leigh syndrome, a neurodegenerative disorder associated with mitochondrial dysfunction, by restoring mitochondrial bioenergetics in neurons<sup>20</sup>. However, the therapeutic potential and underlying molecular mechanism of mitochondria transplantation for treating CBND remain to be fully elucidated.

Our study reveals that Drp1 knockout-induced Purkinje cell degeneration drives ataxia through increased mitophagy and apoptosis, as well as activation of surrounding astrocytes and microglia. However, upregulation of Drp1 in cerebellar PCs failed to attenuate progressive Purkinje cell loss and motor dysfunction. Crucially, we showed that early-stage intracerebellar administration of exogenous healthy mitochondria in cerebellar neurodegenerative mice significantly inhibited progressive Purkinje cell loss and behavioral impairment. These findings position PCs and mitochondrial function status as key indicators for ameliorating cerebellar neurodegeneration, highlighting mitochondria transplantation as a promising therapeutic approach for early-stage cerebellar neurodegeneration.

## Results

### Generation of cerebellar neurodegeneration model (CBND) by conditional knock-out of Drp1 in Purkinje cells (PCKO)

Based on previous studies<sup>21</sup>, we generated Drp1<sup>fllox/flox</sup>;Pcp2-Cre mice (Fig. 1a and Supplementary Fig. 1) whose Drp1 gene was specifically knocked out in cerebellar PCs (PCKO), also named CBND<sup>general</sup> mice. Their wild-type (WT) littermates were used as the control. Both PCKO and control mice were viable, fertile, and exhibited normal in size and weight (Fig. 1b). Over the course of 1 year, no significant death was observed in PCKO mice. Despite severe balance dysfunction, 1-year-old PCKO mice were still able to move freely (Supplementary Movie 1). Three-month-old (3M) PCKO mice exhibited substantial cerebellar atrophy (Fig. 1c). Immunofluorescence staining with Calbindin revealed a significant reduction in the number of PCs in the 3M PCKO mice (Fig. 1d, e). The sagittal planes of the mouse cerebellum (1–4 M) were subjected to immunofluorescence staining using Calbindin, GFAP (an astrocyte marker) and IBA1 (a microglia marker) (Supplementary Fig. 2a). The number of PCs in CBND<sup>general</sup> mice was decreased progressively over time: to 22.55% at 2 months, to 6.19% at 3 months, and to 3.55% at 4 months, compared with 3-month-old WT control mice (Fig. 1f). And the thickness of the molecular layer (ML) in CBND<sup>general</sup> mice also decreased sharply starting at 2 months of age (Fig. 1g). Accompanying the progression of PCs loss, the intensity of GFAP (Supplementary Fig. 2b) and IBA1 (Supplementary Fig. 2c) gradually and significantly increased starting at 1 month of age. Next, immunofluorescent staining and RNAscope experiment showed that DRP1 protein and Drp1 mRNA both reduced obviously in PCs of PCKO mice at 3 months old (Fig. 1h–j).

Furthermore, we performed behavioral tests to detect the motor function of PCKO mice, including gait analysis, rotarod tests and balance beam tests. Compared to WT mice at 3 months of age, PCKO mice exhibited a swaying gait at the same age (Fig. 1k). The results of rotarod test indicated that PCKO mice developed impaired coordination as early as 4 weeks of age, with symptoms progressively worsening over time (Fig. 1l). Balance beam tests showed PCKO mice exhibited impaired balance at the age of 6 weeks (Fig. 1m).

These findings demonstrate that PCKO mice present cerebellum atrophy, PCs neurodegeneration, and progressive ataxia. Additionally, motor dysfunction and glial activation tend to occur earlier than PCs loss.

### Generation of TdTomato-expressing CBND (CBND<sup>TdTomato</sup>) by TdTomato knock-out mice (PC<sup>TdTomato</sup>KO)

In order to ensure the stability of the experiment and exclude the non-characteristic interference from immunofluorescence staining, we constructed PC<sup>TdTomato</sup>KO mice in which cerebellar PCs genetically expressed TdTomato protein (Supplementary Fig. 3a, b), also named TdTomato-expressing CBND (CBND<sup>TdTomato</sup>) mice. The middle sagittal planes were analyzed, revealing that PCs began to degenerate at 2 months old (Supplementary Fig. 3c, d). Similarly, the cerebellum area on the middle sagittal plane showed signs of atrophy beginning at 2 months old (Supplementary Fig. 3e). And the PCs in PC<sup>TdTomato</sup> mice showed no distinction between 1, 2, 3, and 4 months old (Supplementary Fig. 4). Based on the behavioral results from PCKO mice, we conducted rotarod and balance beam tests on 1-month-old PC<sup>TdTomato</sup>KO mice, who similarly exhibited ataxia (Supplementary Fig. 3f, g). Pearson correlation analysis was conducted to explore the relationship between PCs and motor behavior, showing that the number of PCs was negatively correlated with hindfoot slips (Supplementary Fig. 3h).

Based on these results, it can be inferred that motor dysfunction can be reversibly alleviated before significant loss of PCs. Specifically, therapeutic interventions at an early stage of mouse development, such as 1 month of age, may delay the progression of cerebellar neurodegeneration.

### Targeted overexpression of Drp1 in PCs failed to rescue ataxia in adolescent Drp1-PCKO mice

We designed gain-of function experiments (Supplementary Fig. 5a) to investigate whether Drp1 supplement in PCs could ameliorate ataxia in 1-month-old CBND<sup>general</sup> mice. The 1M PCKO mice were intracerebellar injected with Drp1-DIO-OE virus. After 4 weeks, the virus was widely expressed in the cerebellum (Supplementary Fig. 5b), and both Drp1 mRNA (Supplementary Fig. 5c, d) and DRP1 protein levels (Supplementary Fig. 5e, f) were successfully upregulated in the cerebellum of PCKO mice. The rotarod test showed that coordination activity in PCKO mice had no improvement after Drp1-targeted OE treatment (Supplementary Fig. 5g). Similarly, there was no improvement in balance ability in PCKO mice following Drp1 upregulation compared to Drp1 NC treatment (Supplementary Fig. 5h).

Therefore, in the subsequent study, we developed a strategic framework for implementing mitochondria transplantation as a therapeutic approach for cerebellar neurodegeneration.

### Strategy of liver-originated free mitochondria transplantation into the degenerated cerebellum of CBND mice and mitochondrial quality control

Considering the mitochondrial deficit of PCKO mice and the favorable therapeutic effect of mitochondria transplantation on neuronal diseases, we explored the potential of mitochondria transplantation to treat cerebellar neurodegeneration. We injected hepatic-derived mitochondria from WT mice into the cerebellum of PCKO mice (Fig. 2). Healthy mitochondria isolated from 100 mg of liver tissue were stained with Mitotracker to elucidate their bioactive functions (Fig. 2a–d). It was observed that the isolated mitochondria exhibited vivid red Mitotracker fluorescence, indicating the preservation of intact bioactive functions (Fig. 2d). The VDAC1 protein results further confirmed the presence of mitochondria (Fig. 2e).

To verify the purity of the isolated mitochondria, we extracted mitochondrial proteins and assessed potential contamination through detection of extracellular vesicles markers (CD81, CD63, CD9) and cytoplasmic proteins marks (GAPDH). The results showed that the

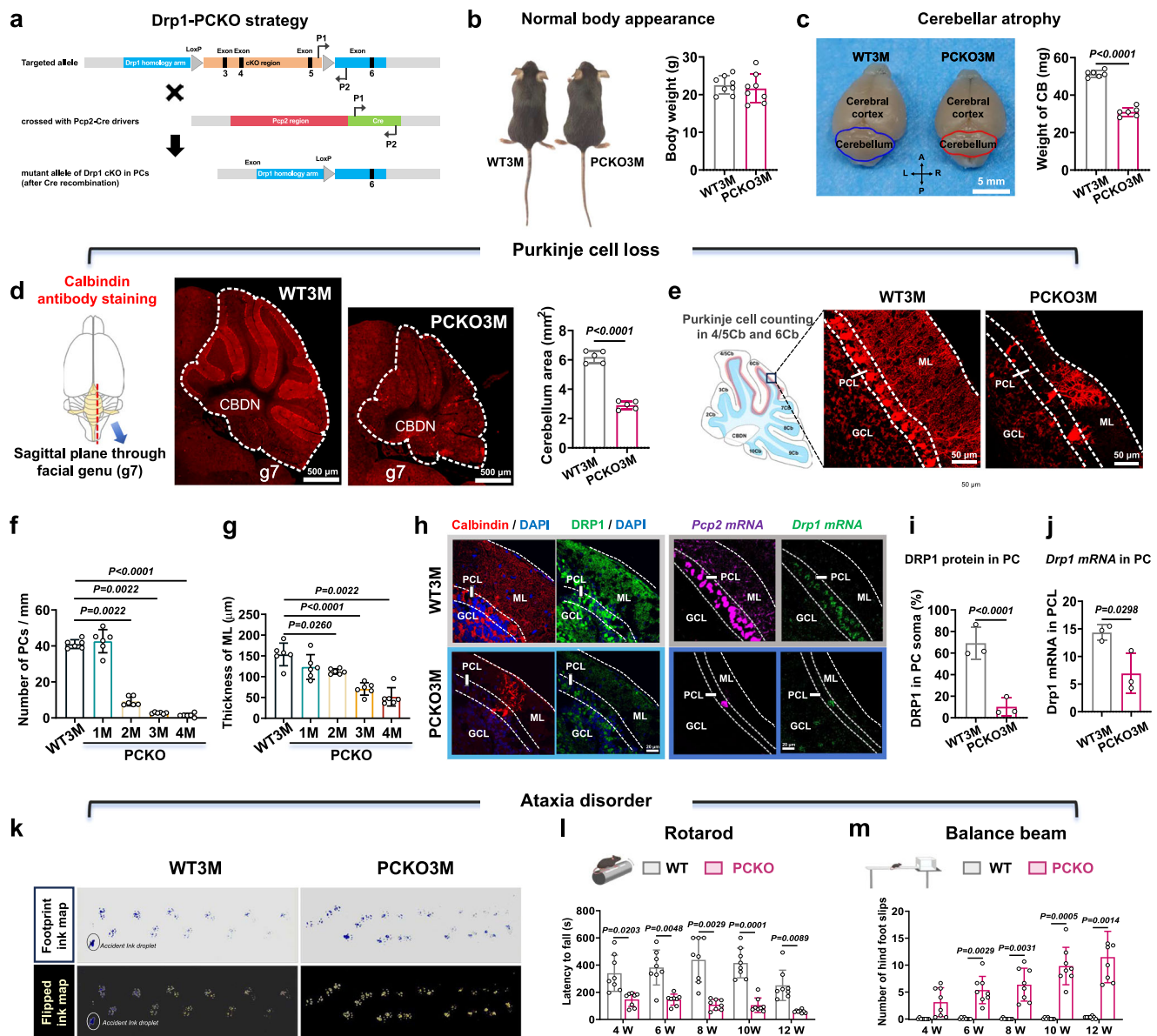


**Fig. 1 | Generation of a cerebellar neurodegeneration model (CBND) in mice by the conditional knock-out of Drp1 gene from Purkinje cells (PCKO).** **a** The construction strategy for a CBND mouse model generated by knock-out of the Drp1 in Purkinje cells. **b** Phenotypic characteristics and quantification of body weight. Two-tailed unpaired *t* test; *n* = 8 mice. **c** Macroscopic appearance and quantification of cerebellar weight. Scale bar = 5 mm. Two-tailed unpaired *t* test; *n* = 6 mice. **d** Confocal images and quantification of Calbindin staining (Red) in the cerebellum. Scale bars = 500  $\mu$ m. Two-tailed unpaired *t* test; *n* = 5 mice. **e** Calbindin staining (Red) in the 6Cb. Scale bars = 50  $\mu$ m. *n* = 5 mice. **f** Quantification of the number of Purkinje cells (PCs). Two-tailed unpaired *t* test; *n* = 6 (3 mice, 2 technical replicates). **g** Quantification of the ML thickness. Two-tailed unpaired *t* test or Mann-Whitney U test; *n* = 6 (3 mice, 2 technical replicates). **h** Immunofluorescence images of

Calbindin (Red) and DRP1 protein (Green). RNAscope image of Pcp2 (Purple) and Drp1 mRNA (Green). Scale bars = 20  $\mu$ m. **i** Quantification of DRP1 protein levels in the soma of PCs. Two-tailed unpaired *t* test; *n* = 3 mice. **j** Quantification of Drp1 mRNA levels in the soma of PCs. Two-tailed unpaired *t* test; *n* = 3 mice. **k** Footprint images of 3-month-old WT and PCKO mice. **l** Quantification of the latency to fall. Two-way ANOVA test and Sidak test; *n* = 8 mice. **m** Quantification of the number of hind foot slips. Two-way ANOVA test and Sidak test; *n* = 8 mice. The data was shown by mean  $\pm$  SD. Cartoon images were created in BioRender. Li, S. (2025) <https://BioRender.com/j40j862>. A anterior, CB cerebellum, Cb cerebellar lobule, GCL Granule cell layer, L left, M Month, ML molecular layer, P posterior, PCL Purkinje cell layer, Pcp2 Purkinje cell protein 2, R right, WT wild type.

expression levels of these proteins in isolated mitochondria suspension were significantly reduced relative to liver homogenate controls (Supplementary Fig. 6a). To evaluate the integrity of both inner and outer membranes, we analyzed the expression levels of TOM20, VDAC1, and SDHB. The results demonstrated that the expression levels of these proteins in isolated mitochondria showed no significant differences compared to those in liver tissues (Supplementary Fig. 6b). Furthermore, our analysis detected minimal DRP1 expression in the isolated mitochondrial fraction, thereby excluding potential functional interaction between DRP1 and mitochondria during the isolation

procedure (Supplementary Fig. 6c). Additionally, electron microscopy was utilized to examine the ultrastructure of the isolated mitochondrial fractions. Supplementary Fig. 6d confirmed the structural preservation of both inner and outer mitochondrial membranes. Notably, the mitochondrial preparations consisted of discrete entities devoid of extracellular vesicle encapsulation. Statistical analysis revealed that the average surface area of individual mitochondrion was  $-0.4103 \pm 0.1653 \mu\text{m}^2$ . Importantly, while the suspension contained non-mitochondrial particulates, these exhibited marked structural degeneration and lacked identifiable organelle features.



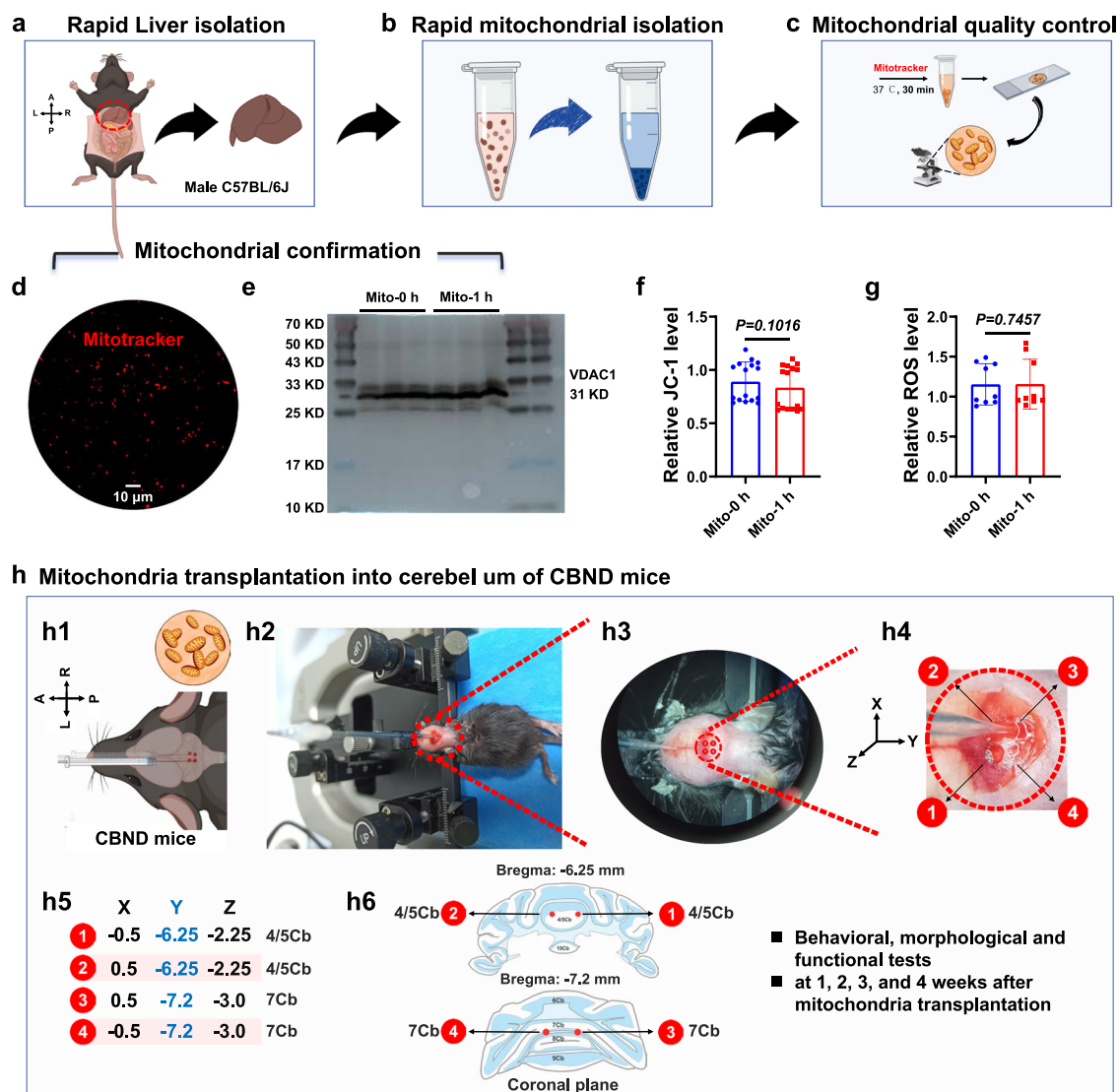


**Fig. 2 | Transplantation of liver-derived healthy mitochondria into the degenerated cerebellum of CBND mice and associated mitochondrial quality control.** **a** Rapid isolation of the liver from a male C57BL/6J mouse. **b** Rapid isolation of mitochondria from the liver tissue. **c** Mitochondrial quality control assessed by Mitotracker Red staining. **d, e** Mitochondrial quality confirmation by Mitotracker observation under confocal microscope (Scale bar = 10  $\mu$ m) (**d**) and Western Blot analysis of VDAC1 ( $n = 3$  mice) (**e**). **f** Quantification of mitochondrial membrane potential levels using JC-1 fluorescence in isolated mitochondria at 0 or 1 h post-

isolation. Two-sided Mann-Whitney  $U$  test;  $n = 16$  (4 mice, 4 technical replicates). **g** Quantification of ROS levels using DCFH-DA fluorescence in isolated mitochondria at 0 or 1 h post-isolation. Two-sided Mann-Whitney  $U$  test,  $n = 9$  (3 mice, 3 technical replicates). **h** The process of mitochondria transplantation into the cerebellum of CBND<sup>general</sup> mice. The data was shown by mean  $\pm$  SD. Cartoon images were created in BioRender. Li, S. (2025) <https://BioRender.com/j40j862>. A anterior, CBND cerebellar neurodegeneration, Cb cerebellar lobule, h hour, L left, Mito mitochondria, P posterior, R right.

Finally, we measured the mitochondrial membrane potential (MMP), ROS level and electron respiratory chain (Complex I, Complex II, Complex III, Complex IV, and Complex V) activity in isolated mitochondria (Supplementary Fig. 6e, f). The results indicated that the functional integrity of isolated mitochondria remained comparable to native hepatic mitochondria in situ. Given the vulnerability of mitochondria, we controlled the process of mitochondria transplantation process to within 1 h. We conducted protein extraction from liver-derived mitochondria at 0 and 1 h post-isolation and evaluated the MMP using JC-1 staining and ROS levels using DCFH-DA. The results demonstrated that both MMP and ROS levels remained unchanged within 1 h after extraction (Fig. 2f, g).

Notably, we detected region-specific PCs loss across cerebellar sagittal sections in CBND mice, which revealed significantly higher neuronal loss in the vermis compared to cerebellar hemispheres at 2 months postnatal (Supplementary Fig. 7). Based on these findings, mitochondria transplantation in CBND mice was stereotactically targeted to four

coordinates within the cerebellar vermis. Freshly isolated mitochondria (50 mg protein/mL) were bilaterally administered via stereotaxic microinjection, with two rostral sites ( $\pm 0.5$  mm,  $-6.25$  mm,  $-2.25$  mm) corresponding to lobule 4/5 Cb and two caudal sites ( $\pm 0.5$  mm,  $-7.2$  mm,  $-3.0$  mm) localized to lobule 7Cb, as anatomically defined in Mouse Brain Atlas (3rd edition) and schematized in Fig. 2h.

### Mitochondria transplantation significantly alleviated neuron loss and ataxia disorder during adolescence in both CBND<sup>general</sup> mice and CBND<sup>TdTomato</sup> mice, but not in adult CBND<sup>general</sup> mice

After mitochondria transplantation at 1, 2, 3, and 4 weeks, the CBND<sup>general</sup> mice underwent balance beam tests (Fig. 3a). Notably, the CBND<sup>general</sup> mice administered mitochondria transplantation at 1 month of age (CBND<sup>general</sup> + Mito) exhibited enhanced motor performance 3 weeks post-intervention, demonstrating rapid beam traversal with stable hindlimb coordination (Fig. 3b and Supplementary



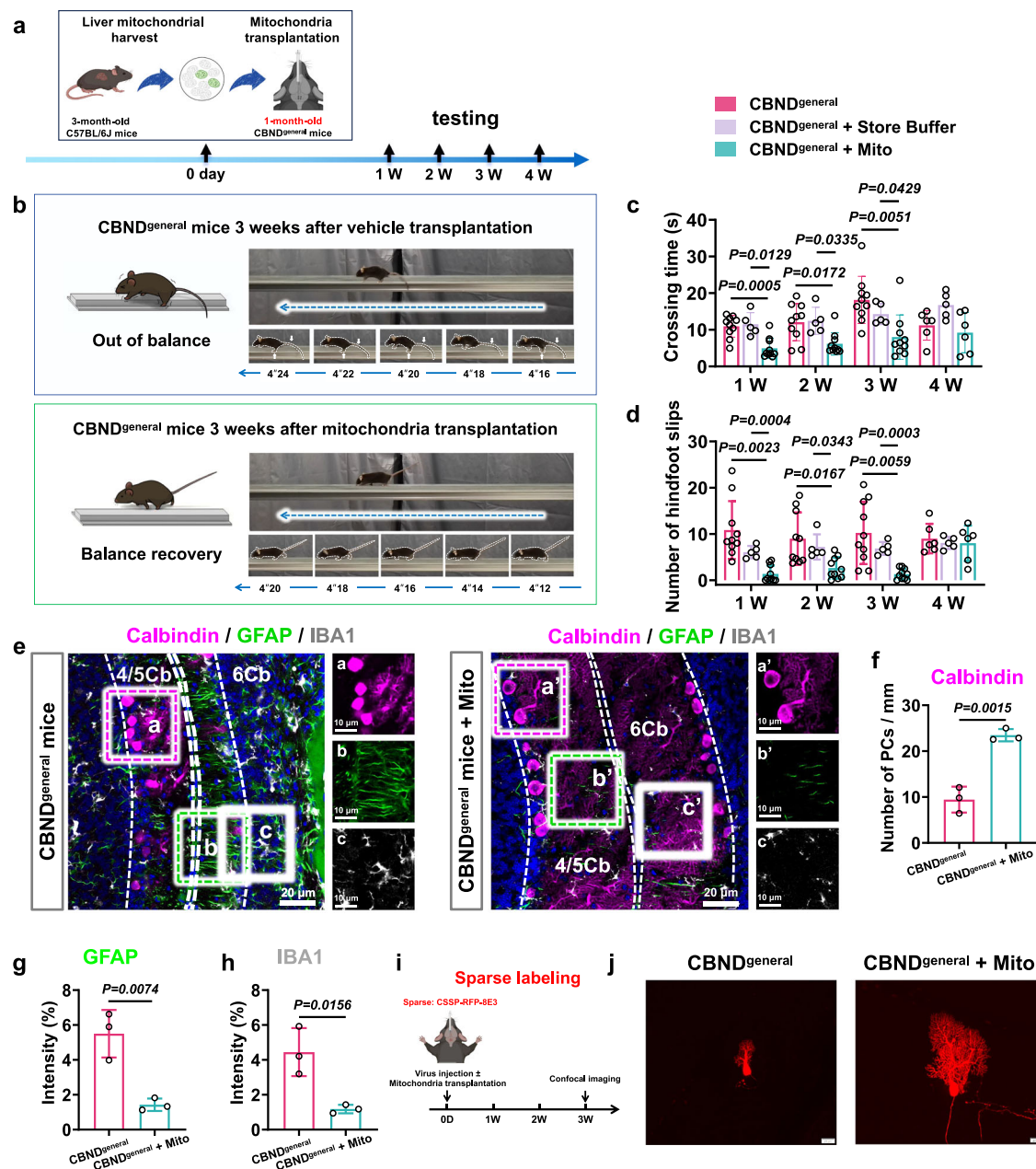


**Fig. 3 | Significant alleviation of neuronal loss and ataxia in early-stage CBND<sup>general</sup> mice following mitochondria transplantation.** **a** Schematic of mitochondria transplantation into 1-month-old CBND<sup>general</sup> mice. **b** Performances of vehicle-treated (upper panel) and Mito-treated (lower panel) CBND<sup>general</sup> mice on the balance beam 3 weeks post-treatment. Quantification of crossing time (**c**) and the number of hindfoot slips (**d**) on the balance beam for CBND<sup>general</sup> mice without treatment, with store buffer treatment, or with mitochondria transplantation 1, 2, 3, and 4 weeks post-treatment. Two-way ANOVA test and Sidak test.  $n = 10$  mice for CBND<sup>general</sup> and CBND<sup>general</sup> + Mito group 1, 2, and 3 weeks post-treatment.  $n = 6$  mice for CBND<sup>general</sup> and CBND<sup>general</sup> + Mito group 4 weeks post-treatment.  $n = 5$  mice for CBND<sup>general</sup> + Store Buffer group. **e** Sagittal confocal images of Purkinje cells (stained with Calbindin in purple), astrocytes (stained with GFAP in green) and microglia

(stained with IBA1 in white) in Cb4/5 and Cb6 of CBND<sup>general</sup> mice with or without mitochondria transplantation 3 weeks post-treatment. Scale bars = 20 μm or 10 μm.  $n = 3$  mice. Quantification of the number of Calbindin-stained Purkinje cells (PCs) (**f**), the intensity of GFAP-stained astrocytes (**g**), the intensity of IBA1-stained microglia (**h**) in CBND<sup>general</sup> mice with or without mitochondria transplantation. Two-sided Mann-Whitney  $U$  test.  $n = 3$  mice. **i** Schematic of sparse imaging for CBND<sup>general</sup> mice with or without mitochondria transplantation. **j** Confocal images of sparse imaging. Scale bars = 20 μm.  $n = 3$  mice. The data was shown by mean  $\pm$  SD. Cartoon images were created in BioRender. Li, S. (2025) <https://BioRender.com/j40j862>. CBND cerebellar neurodegeneration, Cb cerebellar lobule, GFAP Glial fibrillary acidic protein, IBA1 Ionized calcium binding adapter molecule 1, Mito mitochondria, W weeks.

Movie 2). Statistical analysis confirmed significant improvements in motor coordination in CBND<sup>general</sup> + Mito mice at 1, 2, and 3 weeks post-transplantation, as evidenced by reduced crossing time (Fig. 3c) and hindfoot slips (Fig. 3d), compared with both CBND<sup>general</sup> mice and CBND<sup>general</sup> + Store Buffer mice. The therapeutic effect maintained statistically significant through week 3 post-transplantation but faded away in the week 4 (Fig. 3c, d). We further identified GFAP-positive

astrocytes and IBA1-positive microglia in the cerebellum (Fig. 3e). Compared with the CBND<sup>general</sup> group, CBND<sup>general</sup> + Mito mice showed significantly reduced numbers of GFAP- and IBA1-positive cells, along with well-preserved PCs, at 3 weeks post-mitochondria transplantation (Fig. 3e–h). Moreover, cerebellar administration of a sparse viral tracer demonstrated that mitochondria transplantation delayed progression of PCs degeneration in CBND<sup>general</sup> mice relative to controls (Fig. 3i, j).

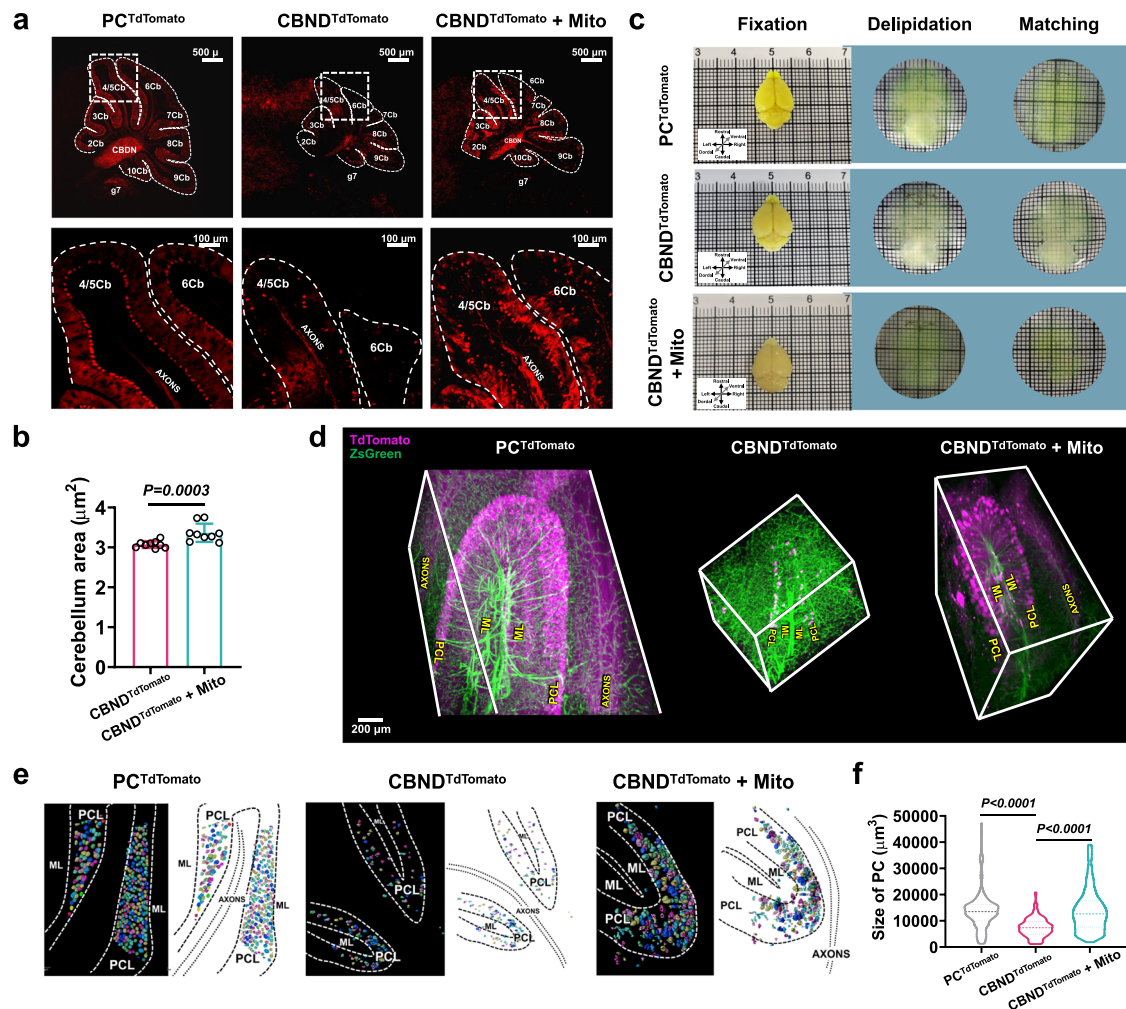


**Fig. 4 | Significant alleviation of neuronal loss in early-stage CBND<sup>TdTomato</sup> mice following mitochondria transplantation.** **a** Sagittal confocal images of Purkinje cells in PC<sup>TdTomato</sup> mice (control), CBND<sup>TdTomato</sup> mice and CBND<sup>TdTomato</sup> mice with mitochondria transplantation (CBND<sup>TdTomato</sup> + Mito). Scale bars = 500  $\mu\text{m}$  (top) and 100  $\mu\text{m}$  (bottom).  $n = 3$  mice. **b** Quantification of cerebellar area in CBND<sup>TdTomato</sup> mice and CBND<sup>TdTomato</sup> + Mito mice. Two-sided Mann-Whitney  $U$  test;  $n = 9$  (3 mice, 3 technical replicates). **c** CUBIC tissue clearing of PC<sup>TdTomato</sup> mice, CBND<sup>TdTomato</sup> mice, and CBND<sup>TdTomato</sup> + Mito mice. **d** Three-dimensional images of the CUBIC-cleared cerebellum from PC<sup>TdTomato</sup> mice, CBND<sup>TdTomato</sup> mice, and CBND<sup>TdTomato</sup> + Mito mice.

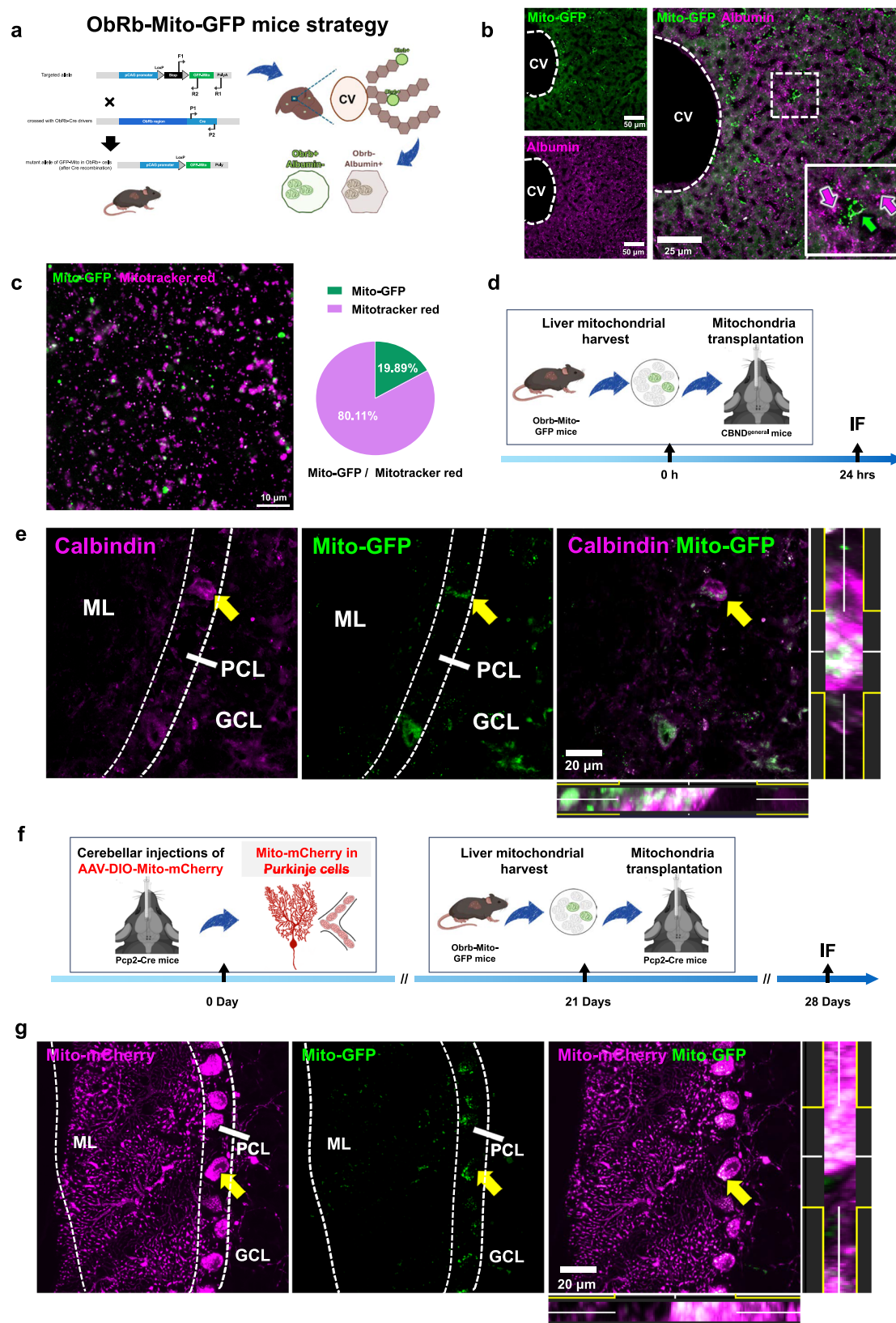
Scale bar = 200  $\mu\text{m}$ .  $n = 3$  mice. **e** Imaris images of Purkinje cells in the Purkinje cell layer (PCL) of the cerebellum from PC<sup>TdTomato</sup> mice, CBND<sup>TdTomato</sup> mice, and CBND<sup>TdTomato</sup> + Mito mice.  $n = 3$  mice. **f** Quantification of size of Purkinje cell (PC) soma in PC<sup>TdTomato</sup> mice, CBND<sup>TdTomato</sup> mice, and CBND<sup>TdTomato</sup> + Mito mice. One-way Kruskal-Wallis test and Dunnett's  $t$  test;  $n = 288$  somas in PC<sup>TdTomato</sup> group, 200 somas in CBND<sup>TdTomato</sup> group, and 735 somas in CBND<sup>TdTomato</sup> + Mito group (3 mice each group). The data was shown by mean  $\pm$  SD. CBND cerebellar neurodegeneration, Mito mitochondria, ML molecular layer, PC Purkinje cell, PCL Purkinje cell layer.

Based on the confocal images of mid-sagittal sections from PC<sup>TdTomato</sup> mice, CBND<sup>TdTomato</sup> mice, and CBND<sup>TdTomato</sup> + Mito mice (Fig. 4a), quantitative cerebellar areas analysis revealed a significant amelioration of cerebellar atrophy in CBND<sup>TdTomato</sup> + Mito mice compared to that in CBND<sup>TdTomato</sup> mice (Fig. 4b). To explore the effects of mitochondria transplantation on the whole cerebellum, we conducted CUBIC brain clearing experiments on cerebella isolated from PC<sup>TdTomato</sup> mice, CBND<sup>TdTomato</sup> mice, and CBND<sup>TdTomato</sup> + Mito mice (Fig. 4c). The number of PCs in CBND<sup>TdTomato</sup> + Mito mice significantly increased, and the dendritic arbors remained robustly developed when observed under a light-sheet microscope (Fig. 4d). The light-sheet microscopy was performed to acquire images of PC<sup>TdTomato</sup> mice (Supplementary Movies 3 and 6), CBND<sup>TdTomato</sup> mice (Supplementary Movies 4 and 7), and CBND<sup>TdTomato</sup> + Mito mice (Supplementary Movies 5 and 8). Imaging was conducted in the sagittal plane from the edge to the mid-sagittal sections (Supplementary Fig. 8) and in the coronal plane from posterior to anterior (Supplementary Fig. 9). Through the segmentation process (Fig. 4e), the size of PC showed a significant improvement in CBND<sup>TdTomato</sup> + Mito mice compared with CBND<sup>TdTomato</sup> mice, with

values returning to levels comparable to those observed in PC<sup>TdTomato</sup> mice (Fig. 4f).

To investigate whether mitochondria transplantation confers therapeutic benefits in adult CBND<sup>general</sup> mice, we observed the effect of mitochondria transplantation on 2 months (Supplementary Fig. 10a–e) or 3 months of age (Supplementary Fig. 10f–j) CBND<sup>general</sup> mice and conducted behavioral tests 3 weeks post-intervention. Calbindin staining showed that mitochondria transplantation had no therapeutic effect on the number of PCs in adult CBND<sup>general</sup> mice (Supplementary Fig. 10b, c, g, h). Immunostainings of GFAP and IBA1 demonstrated that mitochondria transplantation did not significantly alter the intensity of GFAP- and IBA1-positive cells in adult CBND<sup>general</sup> mice (Supplementary Fig. 10b, g). Similarly, there was no significant difference in coordination or balance ability between CBND<sup>general</sup> mice and mitochondria-treated CBND<sup>general</sup> mice at 2 months (Supplementary Fig. 10d, e) or 3 months of age (Supplementary Fig. 10i, j). These results indicate that an adequate Purkinje cells population is essential for mitochondria transplantation to effectively mitigate Purkinje cell degeneration progression.





### The successful entry and sustained residence of exogenously transplanted mitochondria within the receipt PCs

To verify whether exogenous mitochondria could enter PCs, we crossed Mito-GFP mice with ObRb-Cre mice to generate ObRb-Mito-GFP mice (Fig. 5a), in which the hepatic ObRb+ cells exhibited bright Mito-GFP fluorescence explicitly localized in the mitochondrial

compartment (Fig. 5b). Using Mitotracker red to stain the isolated mitochondria from the liver of ObRb-Mito-GFP mice, we found that ~19.89% were GFP positive (Fig. 5c). We transplanted the liver-derived mitochondria from ObRb-Mito-GFP mice into the cerebellum of 1M CBND<sup>general</sup> mice (Fig. 5d). Twenty-four hours post-transplantation, GFP-labeled exogenous mitochondria were observed within the soma



**Fig. 5 | Enter and residence of exogenous mitochondria into Purkinje cells.**

**a** The construction strategy for the ObRb-Mito-GFP mice whose mitochondria in ObRb positive cells express green fluorescence protein. **b** Confocal images of the liver from the ObRb-Mito-GFP mouse stained with Albumin (Purple). Bars = 50  $\mu$ m or 25  $\mu$ m.  $n = 3$  mice. **c** Confocal image of liver-isolated mitochondria from ObRb-Mito-GFP mice stained with Mitotracker red (Purple). The pie chart showed the proportion of GFP+ mitochondria in liver mitochondria (right). Bar = 10  $\mu$ m.  $n = 3$  mice. **d** The timeline illustrates that C57BL/6J mice were transplanted with mitochondria from ObRb-Mito-GFP mice and were sacrificed 24 h post-transplantation. **e** Sagittal confocal images

demonstrate that exogenous green mitochondria successfully entered Purkinje cells (Calbindin, Purple). Bar = 20  $\mu$ m.  $n = 3$  mice. **f** The timeline shows the mito-mCherry labeled Pcp2-Cre mice were transplanted with mitochondria from ObRb-Mito-GFP mice and were sacrificed 7 days post-transplantation. **g** Sagittal confocal images show that endogenous mCherry-labeled mitochondria colocalized with exogenous green mitochondria. Bar = 20  $\mu$ m.  $n = 3$  mice. The data was shown by mean  $\pm$  SD. Cartoon images were created in BioRender. Li, S. (2025) <https://BioRender.com/j40j862>. GCL Granule cell layer, h hour, hrs hours, IF immunofluorescent staining, Mito mitochondria, ML molecular layer, PCL Purkinje cell layer, Pcp2 Purkinje cell protein 2.

of PCs (Fig. 5e). To investigate whether the exogenous mitochondria could communicate with endogenous mitochondria in PCs, we administered a mitochondria-targeting virus into Pcp2-Cre mice. After 21 days, liver-derived mitochondria from ObRb-Mito-GFP mice were transplanted into the virus-treated Pcp2-Cre mice (Fig. 5f). The results manifested that the exogenous GFP-labeled mitochondria were able to enter and interact with PCs (Fig. 5g).

Furthermore, we observed whether other cells in the cerebellum may also take exogenous mitochondria up. We stained the liver-originated mitochondria from the WT mice with Mitotracker green and then transplanted them into the cerebellum of 1M CBND<sup>general</sup> mice (Supplementary Fig. 11a). The results showed that Mitotracker-labeled mitochondria were detected in PCs, IBA1+, and GFAP+ cells within 1 week post-transplantation, while a large number of mitochondria persisted at the transplantation site (Supplementary Fig. 11b). Longitudinal tracking revealed Mitotracker-labeled mitochondria were predominantly localized to PCs, with minimal presence detected in glial cell populations (Supplementary Figs. 11b and 12).

To address the potential leakage of Mitotracker dye, we further investigated the retention of liver-derived mitochondria in PCs by transplanting GFP-labeled mitochondria from ObRb-Mito-GFP mice into 1M CBND<sup>general</sup> mice (Supplementary Fig. 11a). The retention of exogenous mitochondria in PCs was assessed at 1, 2, 3, and 4 weeks post-transplantation. Confocal microscopy revealed that GFP-labeled exogenous mitochondria were detected within PCs in the 1st week post-transplantation and remained intact for up to 4 weeks (Supplementary Fig. 11c).

### Mitochondria transplantation significantly improved the mitochondrial morphology and function of PCs in adolescent CBND<sup>general</sup> mice

We further investigated whether the liver-originated mitochondria significantly influenced the mitochondria function and morphology in recipient PCs in CBND<sup>general</sup> mice. We administered a mitochondria-targeting virus into 1-month-old Pcp2-Cre mice, CBND<sup>general</sup> mice, and CBND<sup>general</sup> + Mito mice. After 21 days, their cerebella were sectioned for mitochondrial network analysis (MiNA) (Fig. 6a). The MiNA results demonstrated that mitochondria transplantation significantly alleviated the disruption of mitochondrial networks in CBND<sup>general</sup> mice (Fig. 6a). Furthermore, we isolated cerebellar mitochondria to assess mitochondrial function in PCs from Pcp2-Cre mice, CBND<sup>general</sup> mice, and CBND<sup>general</sup> + Mito mice. The analysis results demonstrated that mitochondria transplantation significantly increased ATP levels, enhanced mitochondrial membrane potential (using TMRM dye), and reduced mitochondrial ROS production (using MitoSox dye) in cerebellum of CBND<sup>general</sup> mice (Fig. 6b). To assess respiratory complex activities, we examined the protein levels of Complex I (CI), Complex II (CII), Complex III (CIII), and Complex V (CV). The results demonstrated that mitochondria transplantation significantly mitigated the decline of CIII and CV in CBND<sup>general</sup> mice (Fig. 6c).

### Mitochondria transplantation alleviated Caspase3-mediated apoptosis and Parkin-dependent mitophagy

We investigated whether the effectiveness of mitochondria transplantation in CBND<sup>general</sup> mice could be attributed to DRP1 recovery in

the Purkinje cells. Co-staining of Calbindin and DRP1 showed that mitochondria transplantation did not upregulate DRP1 levels in PCs (Supplementary Fig. 13).

Furthermore, a significant reduction in mRNA levels of ataxia-related molecules, including SCA1 (ATXN1), SCA6 (CACNA1A), SCA7 (ATXN7) and SCA17 (TBP), was observed in the cerebella of 1M CBND<sup>general</sup> mice compared to age-matched WT control mice using RT-qPCR (Fig. 7a). Next, Western blot analysis (Fig. 7b) confirmed a significant reduction in the expression levels of mitochondrial dynamics-related proteins (FIS1 and MFF) and the mitochondrial antioxidant factor SOD1 in the cerebellum of 1M CBND<sup>general</sup> mice. Notably, no differences were observed in phosphorylated DRP1, such as DRP1<sup>S616</sup> and DRP1<sup>S637</sup>, compared to controls.

Using immunofluorescent staining, we further investigated the underlying molecular mechanisms through which mitochondria transplantation ameliorates PCs degeneration (Fig. 7c). We observed a significant increase in Caspase3 (Fig. 7d) and PARKIN (Fig. 7h) expression levels, along with a marked decrease in COX4 levels (Fig. 7f), in PCs of CBND<sup>TdTomato</sup> mice compared to controls. Furthermore, mitochondria transplantation significantly reversed the alterations in Caspase3 (Fig. 7e), COX4 (Fig. 7g), and PARKIN (Fig. 7i) expression. To confirm the influence of mitochondria transplantation on mitophagy, we detected the additional molecules associated with mitophagy. Statistical analysis revealed that mitochondria transplantation significantly mitigated LC3B upregulation (Supplementary Fig. 14a). A significant elevation in PINK1 levels (Supplementary Fig. 14b) was observed in CBND<sup>TdTomato</sup> mice only at 4 months of age, while BNIP3L (Supplementary Fig. 14d) and FUNDC1 (Supplementary Fig. 14e) were significantly elevated only at 3 months of age. No statistically significant difference was found in BNIP3 levels between CBND<sup>TdTomato</sup> mice and control mice (Supplementary Fig. 14c). Furthermore, mitochondria transplantation did not alter the expression levels of PINK1, BNIP3, BNIP3L, or FUNDC1 (Supplementary Fig. 14).

### Mitochondria that lack DRP1 or respiratory capacity could not alleviate behavior abnormality of CBND<sup>general</sup> mice

It was essential to ascertain whether the observed therapeutic effects of mitochondria transplantation could be attributed to the functional integrity of exogenous mitochondria. Consequently, we pretreated liver-derived mitochondria by administering the DRP1 inhibitor Mdivi-1 (Supplementary Fig. 15) or mitochondrial respiratory blocker Carbonyl cyanide 4-(trifluoromethoxy)phenylhydrazone (FCCP) (Supplementary Fig. 16). Then we transplanted them into the cerebellum of CBND<sup>general</sup> mice.

Mdivi-1 or DMSO were administered via intraperitoneal injections to C57BL/6J mice (Supplementary Fig. 15a). Western blot analysis showed reduced DRP1 and Complex V levels in the liver of Mdivi-1-treated mice compared to DMSO-treated or untreated controls (Supplementary Fig. 15b). In addition, mitochondrial ROS production significantly increased, while MMP remained unchanged (Supplementary Fig. 15c). Subsequently, liver mitochondria isolated from Mdivi-1- or DMSO-treated mice were transplanted into the cerebellum of CBND<sup>general</sup> mice. Behavioral analysis revealed significant improvements in balance ability in CBND<sup>general</sup> + DMSO-Mito mice at 1, 2, and 3 weeks post-transplantation compared to CBND<sup>general</sup> mice

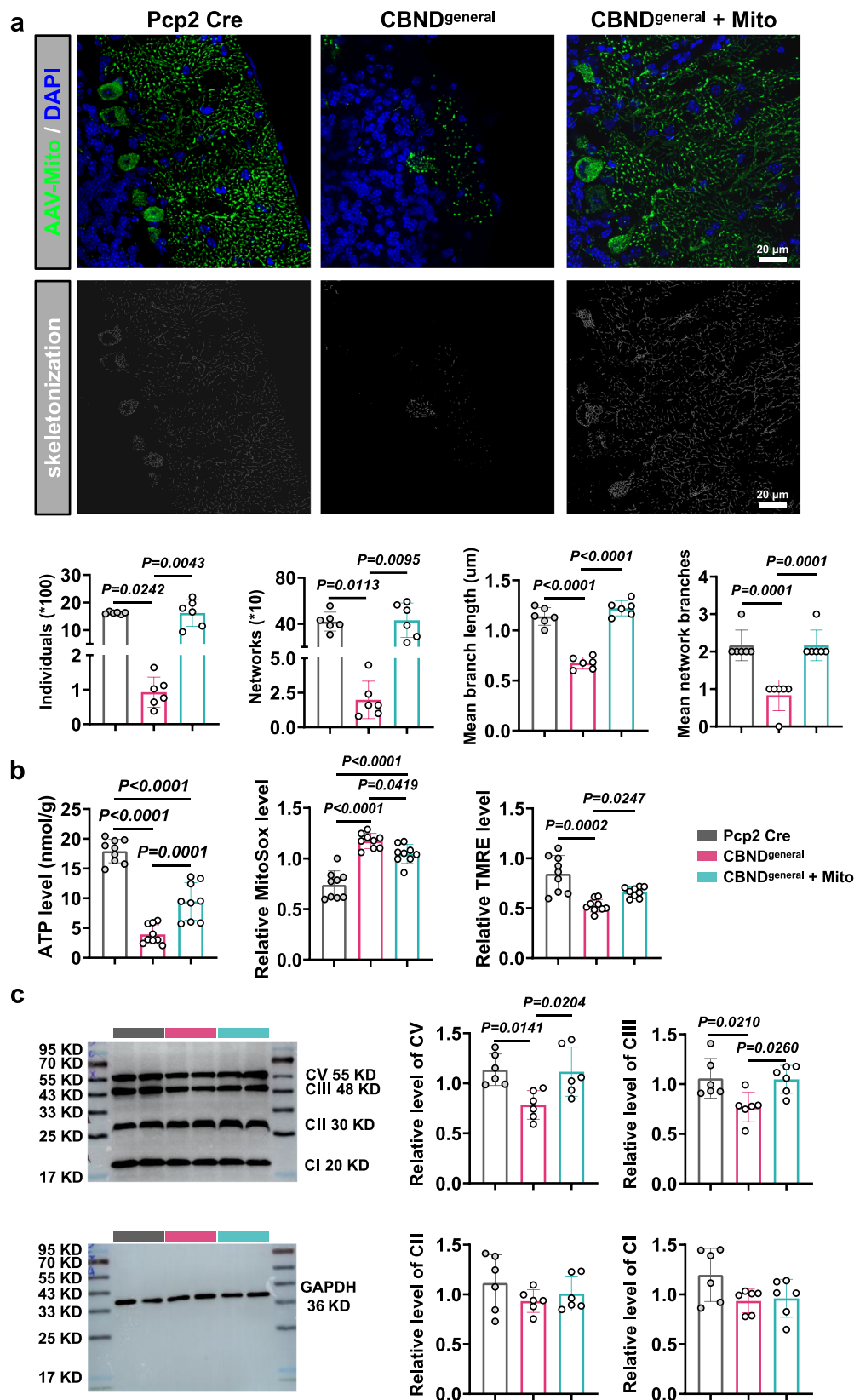


**Fig. 6 | Mitochondria transplantation significantly improve the mitochondrial morphology and function of Purkinje cells in CBND<sup>general</sup> mice.** **a** MiNA analysis tested from Pcp2 Cre, CBND<sup>general</sup>, and CBND<sup>general</sup> + Mito mice at 3 weeks after mitochondria transplantation. One-way ANOVA and Dunnett's *t* test,  $n = 6$  (3 mice, 2 technical replicates). Bars = 20 μm. **b** Results of cerebellar ATP, MitoSox, and TMRE level tested at 3 weeks after mitochondria transplantation. One-way ANOVA and

Dunnett's *t* test,  $n = 9$  (3 mice, 3 technical replicates). **c** Western blot result of Complex I (CI), Complex II (CII), Complex III (CIII) and Complex V (CV) tested at 3 weeks after mitochondria transplantation. One-way ANOVA and Dunnett's *t* test,  $n = 6$  (3 mice, 2 technical replicates). The data was shown by mean ± SD. CBND cerebellar neurodegeneration, Mito mitochondria, Pcp2 Purkinje cell protein 2.

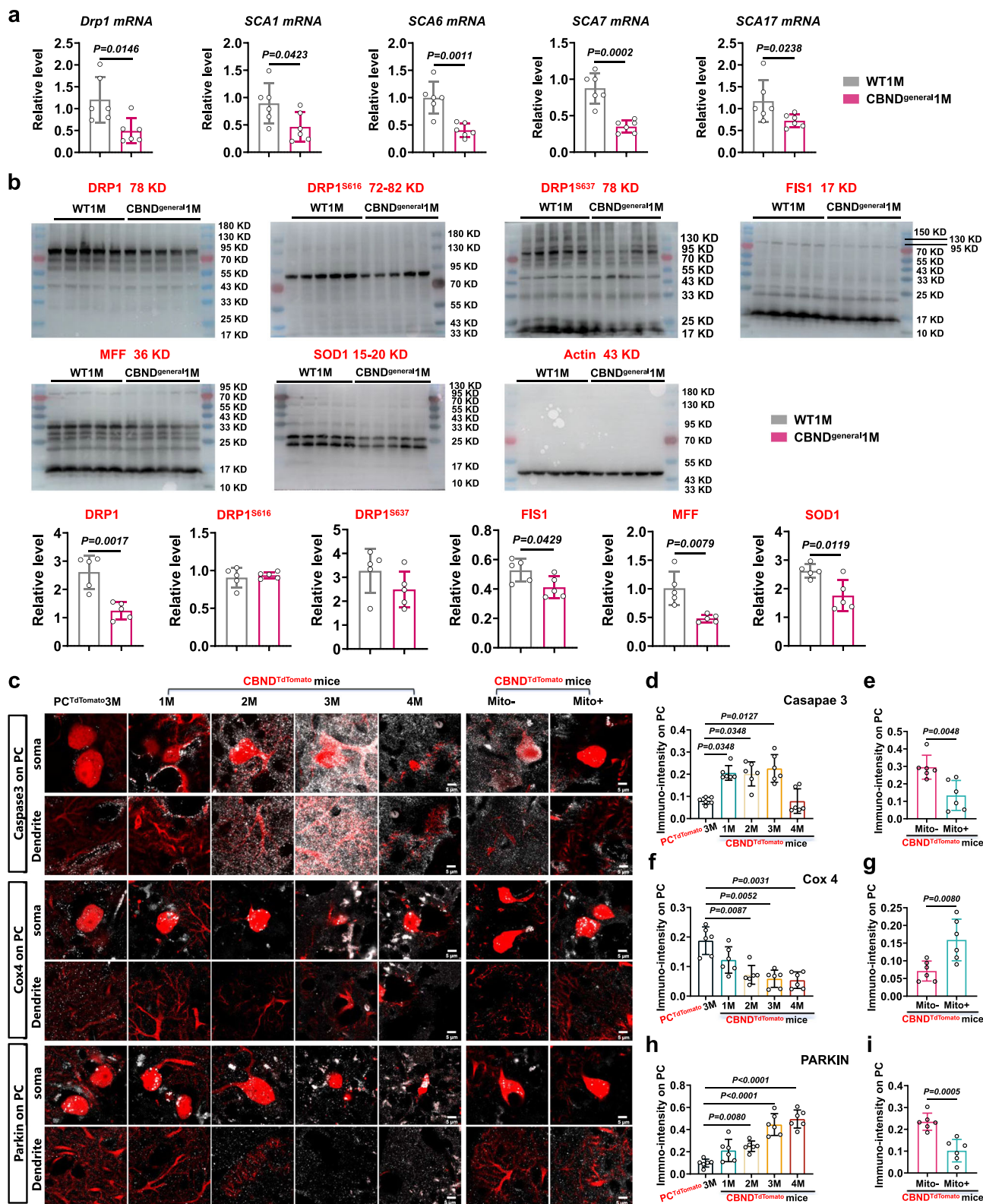


**Fig. 7 | Exogenous mitochondria support degenerated Purkinje cells by inhibiting Caspase3-related cell apoptosis and Parkin-related mitophagy. a** Q-PCR results of *Drp1*, *SCA1*, *SCA6*, *SCA7*, and *SCA17* mRNA from cerebellum of CBND<sup>general</sup> mice tested at 1 month old. Two-tailed unpaired *t* test or Mann-Whitney *U* test,  $n=6$  (3 mice, 2 technical replicates). **b** Western blotting results of DRP1, DRP1<sup>S616</sup>, DRP1<sup>S637</sup>, FIS1, MFF, and SOD from cerebellum of CBND<sup>general1M</sup> mice tested at 1 month old. Two-tailed unpaired *t* test or Mann-Whitney *U* test,  $n=5$  mice. **c** Confocal images of Caspase3, Cox4, and Parkin (White) stained on Purkinje cells (Red) of

CBND<sup>TdTomato</sup> mice at 1-, 2-, 3-, and 4-month-old (left) or on mito-treated CBND<sup>TdTomato</sup> mice (right) 3 weeks post-transplant. Bar = 5  $\mu$ m.  $n=3$  mice. Quantification of Caspase3 (**d**), Cox4 (**f**), and Parkin (**h**) expressing on Purkinje cells of CBND<sup>TdTomato</sup> mice at 1-, 2-, 3-, and 4-month-old. One-way ANOVA and Dunnett's *t* test,  $n=6$  (3 mice, 2 technical replicates). Quantification of Caspase3 (**e**), Cox4 (**g**), and Parkin (**i**) expressing on Purkinje cells of mito-treated CBND<sup>TdTomato</sup> mice (right) 3 weeks post-transplant. Two-tailed unpaired *t* test,  $n=6$  (3 mice, 2 technical replicates). The data was shown by mean  $\pm$  SD. CBND cerebellar neurodegeneration, Mito mitochondria.



(Supplementary Fig. 15d). In contrast, no significant improvement in ataxia was observed in CBND<sup>general</sup> + Mdivi-1-Mito mice at any time points.

Similarly, FCCP or DMSO were administrated to C57BL/6J mice (Supplementary Fig. 16a). Liver mitochondria from FCCP-treated mice exhibited reduced Complex V and MMP levels, along with increased mitochondrial ROS production, compared to controls (Supplementary Fig. 16b, c). Behavioral analysis showed that transplanting FCCP-treated mitochondria into the cerebellum of CBND<sup>general</sup> mice failed to alleviate balance dysfunction (Supplementary Fig. 16d).

These findings demonstrate that mitochondria deficient in DRP1 or respiratory capacity were unable to ameliorate the behavioral abnormalities observed in CBND<sup>general</sup> mice.

## Discussion

Mitochondrial damage is crucial in neurodegeneration, impairing the respiratory chain, mitochondrial DNA, and mitophagy<sup>5</sup>. Therefore, mitochondria-targeted therapies may play a key role in treating neurodegenerative process. In this study, we reported that mitochondria transplantation technology improved mitochondrial function, reduced mitophagy and apoptosis of PCs, thereby delaying cerebellar neurodegeneration. In 2012, Kageyama et al.<sup>21</sup> constructed DRP1-specific knockout mice in PCs, leading to progressive PCs loss. We used this model to study cerebellar neurodegeneration and demonstrated a correlation between PCs degeneration and ataxia symptoms. In the present study, we observed that PCs loss activated astrocytes and microglia, increased apoptosis and mitophagy markers, and impaired mitochondrial function. Additionally, we observed that, while upregulating DRP1 in PCs of PCKO mice did not improve Purkinje cell degeneration or ataxia, injecting liver-derived mitochondria into the cerebellum alleviated apoptosis and mitochondrial dysfunction in PCs, and significantly improved motor impairment.

Previous studies have reported varying concentrations of effective mitochondria across different models. For instance, Nakamura et al. demonstrated beneficial effects of brain mitochondria transplantation with doses ranging from 1 µg to 200 µg<sup>22–24</sup>. In 2017<sup>25</sup>, Kaza et al. transplanted skeletal muscle mitochondria into ischemic heart at doses of  $2 \times 10^5$ ,  $2 \times 10^6$ ,  $2 \times 10^7$ , and  $2 \times 10^8$  mitochondria per gram, founding no significant difference in the infarct size reduction across doses. In 2019<sup>26</sup>, Shin et al. transplanted five concentrations of mitochondria ( $1 \times 10^3$ ,  $1 \times 10^5$ ,  $1 \times 10^7$ ,  $1 \times 10^9$  and  $1 \times 10^{11}$ ) via coronary arteries into transient ischemic heart, showing significantly improvement in myocardial function, perfusion and infarct size at  $1 \times 10^7$ ,  $1 \times 10^9$  and  $1 \times 10^{11}$ , with no significant difference between the doses of  $1 \times 10^9$  and  $1 \times 10^{11}$ . The present study observed that transplantation of 40 µg liver-derived mitochondria significantly alleviated neuron loss and ataxia disorder in adolescent CBND mice. Considering that excessive mitochondrial injection can activate local glial cells<sup>24,27</sup>, we speculate that brain tissue may be damaged by high doses of mitochondria. These studies highlight the necessity of a specific dose threshold for effective mitochondria transplantation and indicate that efficacy does not increase proportionally with higher dose.

The current findings indicate that transplanted mitochondria predominantly accumulate in damaged PCs, although their presence has also been noted in astrocytes and microglia. This raises a question about the selectivity of host cells of transplanted mitochondria. Alexander et al.<sup>28</sup> have reported that nasally delivered mitochondria isolated from human mesenchymal stem cells could be internalized by neurons, macrophages, and GFAP+ cells. Other research has demonstrated that mitochondria from astrocytes<sup>29–31</sup> or microglia<sup>32</sup> can transfer into surrounding impaired neurons to exert neuroprotective effects. Nakai et al.<sup>20</sup> have reported that bone marrow transplantation from wild-type mice significantly improves morbidity and mortality in *Ndufs4*<sup>-/-</sup> mice with Leigh syndrome. This improvement is associated

with the release of extracellular mitochondria derived from haematopoietic cells into circulation and their subsequent transfer to host cells in multiple organs. Additionally, they have also found that administering isolated mitochondria from wild-type mice yields comparable therapeutic effects in Leigh syndrome mice. These data suggest that transplanted mitochondria selectively accumulate in damaged cells including neurons, and mitochondria transplantation-related approaches could be a promising approach for treating ND, such as CBND.

Mitochondria constitute dynamic networks within the cell, maintained through a balanced process of continuous fusion and fission<sup>33,34</sup>. The executor of mitochondrial fission is the GTPase enzyme, specifically referred to as dynamin-related protein 1 (DRP1)<sup>35</sup>. Depletion of DRP1 results in mitochondrial dysfunction<sup>36</sup>. Mitophagy, mediated by PINK1 and Parkin, responds to mitochondrial damage to preserve mitochondrial function<sup>37,38</sup>. Numerous studies indicate that in neurons, when damaged mitochondria fail to be adequately cleared through mitophagy, the accumulation of ROS, nitrogen oxides, and other oxidative agents can lead to the development of various ND<sup>39–41</sup>. Our results have showed that the mitochondrial function was damaged in PCs of CBND mice, indicated by decreased COX4<sup>42,43</sup>, with increased expressions of mitophagy markers (Parkin and LC3B) and Caspase3-related apoptosis<sup>44</sup>. Additionally, mitochondria transplantation has markedly improved mitochondrial function and inhibited both Caspase3-mediated apoptosis and Parkin-dependent mitophagy in PCs of CBND mice. Notably, Lin et al.<sup>19</sup> have demonstrated that mitochondria transplantation enhances recipient cell function by promoting Parkin-mediated mitophagy to clear damaged mitochondria. We propose two key factors that may account for the observed differences. First, the timing of detecting mitophagy marker expression differs between studies. Lin et al. have found the co-localization of DsRed-labeled exogenous mitochondria with cytoplasmic Parkin 24 h post-transplantation. In contrast, our study evaluated the expression of mitophagy markers, including Parkin, LC3B, PINK1, BNIP3, BNIP3L, and FUNDC1, at 21 days post-transplantation in vivo. Second, the role of mitophagy in mitochondria transplantation varies. Lin et al. suggest that transplanted mitochondria initiate mitophagy at an early stage, whereas our findings indicate that transplanted mitochondria rescue mitochondrial function, subsequently restoring mitophagy. These data highlight the critical role of mitophagy in determining the therapeutic efficacy of mitochondria transplantation, indicating that its molecular regulatory mechanisms should be a focal point for future research in this field.

Studies on mitochondria transplantation have generated more questions than answers, primarily due to the unclear mechanisms and variable factors involved. A key unresolved question is whether functional recovery is influenced by the different mitochondrial internalization mechanisms or the interaction between exogenous and endogenous mitochondria in host cells remains to be fully elucidated. Nicolas-Avila et al.<sup>45</sup> have reported that macrophages degrade cardiomyocyte-derived mitochondria within a few days. However, Chang et al.<sup>18</sup> have demonstrated that the signal from transplanted mitochondria remain detectable in recipient neurons for up to 12 weeks post-transplantation. Our current results reveal that GFP-labeled transplanted mitochondria persist in PCs for up to 4 weeks. These marked temporal and cell-type-specific discrepancies strongly suggest that the exogenous mitochondria in PCs might evade degradation. It remains unclear whether exogenous mitochondria within PCs can communicate with endogenous mitochondria, which needs further study.

It is imperative to acknowledge that addressing the deficiency of Drp1 constitutes our most significant challenge. Previous studies have explored gene therapy as a potential treatment for ND<sup>46,47</sup>. In 2014, Michael S Rafii et al. conducted stereotactic gene delivery of AAV2-NGF in early and middle stage to Alzheimer's patients, demonstrating its

safety and tolerability over 2 years<sup>48</sup>. In 2018, Michael S Rafii et al. performed a trial with 49 patients, which showed no significant difference in efficacy between AAV2-NGF and placebo groups<sup>49</sup>. Gene therapy for congenital genetic defects is also time-sensitive, becoming less effective as patients age<sup>50</sup>. These studies highlight the efficacy in gene therapy outcomes across individuals. Our laboratory attempted to deliver Drp1 overexpressing AAV to the cerebellum. Despite successful delivery, Drp1 overexpression failed to correct the fate of neuronal degeneration. We hypothesize this may be attribute to late intervention or insufficient dosage.

Glial cells play an important role in ND. Consistent with previous research, this study verified that astrocytes and microglia activate before mitochondrial damage and neuronal dysfunction<sup>51</sup>. The findings show that the neurons and surrounding glial cells form a interconnected network. However, the activation of glial cells is a consequence, not a cause, of neuronal damage. When mitochondria transplantation corrected the neuronal state, these activated glial cells returned to their resting state. Therefore, monitoring glial cell status may be a reliable indicator of treatment effectiveness, rather than overestimating their supportive potential.

There are some limitations in this study. Ataxia symptoms appeared in PCKO mice at 1 month of age. Although the number of PCs did not significantly decrease at this time, we speculated that their function was already damaged. However, we did not conduct experiments to verify PCs function. Additionally, the effectiveness of mitochondria transplantation in this study lasted only 3 weeks. In future experiments, we aim to extend this duration to explore the potential of mitochondria transplantation as a long-term therapy for cerebellar neurodegeneration.

## Methods

### Ethics statement

All animal protocols complied with the Animal Care and Use Committee of the Air Force Military Medical University and followed the Guidelines for the Care and Use of Laboratory Animals (permit number IACUC-20190107).

### Animals

We purchased Pcp2-Cre mice from the Jackson Laboratory (America, Stock No: 004146). Drp1<sup>fl/fl</sup> were designed by inserting a loxP site after the sequence of Drp1 (Cyagen, CKOAI5191230RT5, China). ObRb-Cre mice were purchased from Cyagen (CKOCMP-74011-Slc25a27-B6N-VA, China). Rosa26-CAG-LSL-GFP-Mito tag mice (Mito-GFP mice) were characterized by green fluorescent protein in outer mitochondrial membrane (Gempharmatech, cas9-ki (Rosa26), China). B6/JGpt-H11<sup>em1</sup>Cin(CAG-LoxP-ZsGreen-Stop-LoxPtdTomato)/Gpt (B6-G/R) mice (T006163, China) and C57BL/6J Gpt mice were both purchased from GemPharmatech. Drp1<sup>fl/fl</sup> mice were crossed with Pcp2-Cre mice for two generations to generate Pcp2-Cre;Drp1<sup>fl/fl</sup> mice (PCKO mice) as knockout mice. PC<sup>tdTomato</sup> KO mice were constructed by PCKO mice and B6-G/R mice. ObRb-Mito-GFP mice were generated by hybridizing ObRb-Cre mice and Mito-GFP mice. All mice were housed (maximum 5 mice in a cage) with free access to food and water under a 12-h day/night cycle (8 am to 8 pm). Experiments used roughly equal numbers of male and female mice. The abbreviations in this study are shown in Supplementary Table 1.

### Genotyping and confirmation

The mouse genotype was identified using mouse direct PCR kit (TSE014, TSINGKE, China). Incubate the tail samples at 55 °C for 30 min, followed by incubation at 98 °C for 15 min. Subsequently, centrifuge the samples at 12,000 × g for 5 min at 4 °C. The supernatant was used as a template for PCR. The PCR cycling condition were: 94 °C for 3 min, 35 cycles of 94 °C for 30 s for denaturation, 60 °C for 35 s for annealing, and 72 °C for 35 s for extension, and after the 35 cycles with

72 °C for additional extension for 5 min. The primers sequence are shown in Supplementary Data 1. Primers and PCR conditions were designed by Tsingke Biotechnology Co., Ltd.

### Tissue preparation

Mice were anesthetized by isoflurane, and were perfused transcardially with 0.01 M phosphate buffered saline (PBS), followed by 4% paraformaldehyde (PFA) in PBS for fixation. The brains were carefully removed and postfixed overnight at 4 °C in 4% PFA. They were then immersed sequentially in sucrose solution (10%, 20%, and 30% in order) for over 48 h for gradient dehydration. Brain sections were cut at 20 μm for Immunofluorescent staining and 10 μm for RNAscope in situ hybridization using a cryostat (Leica CM1850, Germany). Sections were immediately mounted on glass slides and returned into −20 °C cryostat chamber.

### Immunofluorescent staining

Tissues were washed in PBS, blocked with 3% fetal bovine serum and permeabilized with 0.3% TritonX-100 at room temperature for 30 min. Primary antibodies were incubated at 4 °C for up to 18 h (anti-PARKIN for up to 48 h). The detailed information on antibodies is shown in Supplementary Data 2. The secondary antibodies were diluted in PBS and incubated for 2 h at room temperature. Nucleus were stained with 49,69-diamidino-2-phenylindole dihydrochloride (DAPI) (C1005, Beyotime, China) for 15 min. High-resolution images of section from PCKO mice were acquired using confocal microscopy (FV3000, Olympus, Japan). And Leica Stellaris 5 (German) were used to image PC<sup>tdTomato</sup>KO mice. The results were quantified by ImageJ (Version 1.54 f). For colocalization, we used JACoP plugin to get Manders' Colocalization Coefficients (MCC). The total fluorescence intensity of protein in PCs was denoted as PC<sub>i,colocal</sub>, and PC<sub>i</sub> replaced the total fluorescence intensity of PCs. So the quantification of each protein in PCs was represented as MCC<sub>PC</sub>. The formula of MCC<sub>PC</sub> is 
$$MCC_{PC} = \frac{\sum_i PC_{i,colocal}}{\sum_i PC_i}.$$

### RNAscope in situ hybridization

Tissues were baked at 37 °C for 6 h and then washed with 0.01 M PBS for 5 min. They were treated with hydrogen peroxide (322281, ACD, USA) at room temperature for 10 min, following washing twice in distilled water. Tissues were immersed in the boiled Target Retrieval reagents (322000, ACD, USA) at 97 °C for 10 min, then transferred to the room-temperature distilled water and then to the absolute ethanol for an additional 3 min. After air-drying, we outlined them with a hydrophobic pen (CIRISC PAP pen, I.S. CIRCLE WRITER, Japan). Once hydrophobic boundaries dried, protease III reagent (322281, ACD, USA) was added to cover the whole tissue. Slides were incubated in a preheated HybEZ oven (ACD, USA) at 40 °C for 30 min, followed by washing twice in distilled water. For hybridization, a mixture of two probes was then added to each slide until the tissue was fully covered. Drp1 (ACD, USA) and Pcp2 (ACD, USA) were incubated in a HybEZ oven at 40 °C for 2 h, followed by two 2-min washes in washing buffer (310091, ACD, USA). Subsequently, slides were incubated sequentially in AMP-1, AMP-2, and AMP-3 reagents for 30 min, 30 min, and 15 min, respectively. HRP-C1 and HRP-C2 signals were processed in order. Opal 520 (ASOP520, ASbio, USA) marked the channel 1 probe, and Opal 570 (ASOP570, ASbio, USA) marked the channel 2 probe. Finally, tissues were submerged with DAPI. High-resolution images were captured using confocal microscopy (Zeiss, Germany), and were quantified by ImageJ (Version 1.54 f).

### Behavior tests

Each mouse was grouped and numbered based on genotype by a third person. The experimenters were blinded to mouse genotype. All behavioral experiments were conducted between 6 p.m. and 10 p.m.

For motor coordination assessment, rotarod tests (BZY007, Jiliang, China) started at 4 rpm and increased to 40 rpm within 180 s. Each trial lasted 10 min, with at least a 15-min interval. Mice were trained three times daily for three consecutive days, data were collected on the 4th day. The latency to fall from the rod was recorded.

For balance ability tests, mice were trained for 3 consecutive days, 3 times daily, and data were collected on the 4th day. The latency to cross the beam and the number of hind foot slips were recorded. The hindfoot slips were counted if either the left or right hind paw slipped off the beam<sup>8</sup>.

For foot print collection, the feet of the mice were stained with blue ink. Each mouse was placed on a white sheet and made to walk from start to finish. Trials were terminated if the mouse left the paper from the middle without reaching the end.

### Mitochondria isolation

Mitochondria isolation was performed according to the instruction (SM0020, Solarbio, China). Tissue was rinsed in saline and homogenized in Tris-HCl-based lysis buffer. The homogenization was centrifuged at  $1000 \times g$  for 5 min at 4 °C. The supernatant was transferred to a new tube and centrifuged under the same condition. The secondary supernatant was then centrifuged at  $12,000 \times g$  for 10 min at 4 °C. The pellet was resuspended in Tris-HCl-based wash buffer and centrifuged at  $1000 \times g$  for 5 min at 4 °C. The supernatant was centrifuged at  $12,000 \times g$  for another 10 min at 4 °C. Finally, mitochondria were resuspended in phosphate-based store buffer (PH 7.2–7.4).

### Mitochondria membrane potential detection

For JC-1 detection, isolated mitochondria were complied with the manufacturer's instruction (C2006, Beyotime, China). A 900  $\mu$ L JC-1 working solution was added to 100  $\mu$ L mitochondria suspension. Then add 100  $\mu$ L of them to a 96-well plate for the test. Fluorescence was measured in a Microplate reader (Spark, Tecan, Switzerland) with settings: excitation wavelength, 485 nm; emission wavelength, 590 nm. Total fluorescence per microgram (F/mg) of proteins was calculated and analyzed<sup>52</sup>. In control mouse, this value was set to 1. Each sample's relative fluorescence was indicated as a percentage of the control.

For TMRE experiment (C2001S, Beyotime, China), samples were incubated at 37 °C for 20 min. Fluorescence was measured in a same Microplate reader, with settings: excitation wavelength, 485 nm; emission wavelength, 535 nm. TMRE levels were expressed as a percentage of the F/mg in control mice.

### ROS level assay

The ROS level was detected using the ROS Assay Kit (S0033S, Beyotime, China). Mitochondria were extracted as described previously. DCFH-DA was diluted to 10  $\mu$ M in serum-free medium. The mitochondria suspension (10 to 100  $\mu$ g protein) was incubated with DCFH-DA at 37 °C for 20 min, mixing every 3–5 min, and then were washed three times with serum-free medium. Fluorescence was measured using a Microplate reader (Spark, Tecan, Switzerland) with settings: excitation wavelength, 488 nm; emission wavelength, 525 nm. Total fluorescence per microgram of proteins (F/mg) was calculated and analyzed. In control mouse, this value was set to 1, and each sample's relative fluorescence was expressed as a percentage of the control.

For MitoSox assay (S0061S, Beyotime, China), samples were incubated at 37 °C for 20 min. Microplate reader was set as: excitation wavelength, 510 nm; emission wavelength, 580 nm. The MitoSox level of each sample was indicated as a percentage of the F/mg in control mice.

### ATP detection

Enhanced ATP test kit (S0027, Beyotime, China) was used. The cerebellum was homogenized in lysis buffer and centrifuged at  $12,000 \times g$

for 5 min at 4 °C. The supernatant was collected for ATP determination. 100  $\mu$ L ATP detection solution and 20  $\mu$ L sample were added in a 96-well plate for assay. ATP levels were measured using a Microplate reader (Spark, Tecan, Switzerland). Protein content was detected using BCA reagent. The results were demonstrated as ATP concentration (nmol)/protein quality (g).

### Viral injection

The mice were anesthetized with pentobarbital and fixed on a stereoscopic brain locator (RWD 69100, Shenzhen, China). AAVs were diluted to  $1 \times 10^{12}$  v.g./mL and injected using a microsyringe (RWD 79013, Shenzhen, China). Before removal, the needle remained in the cerebellum for 8–10 min.

For DRP1 up-regulation experiments, the viral constructs were pAAV-CMV-DIO-Drp1-P2A-EGFP (H15088, OBio Technology, China) for up-regulating and AAV-CMV-DIO-EGFP (H5010, OBio Technology, China) as control. The injection sites were: ( $\pm 1.00$ ,  $-6.25$ ,  $-2.25$ ; 1  $\mu$ L) and ( $\pm 1.00$ ,  $-7.2$ ,  $-3.00$ ; 1  $\mu$ L).

For sparse-labeling experiments, the viral sequencing was CSSP-RFP-8E3 (BC-SL005, Braincase, China). The injection sites were: ( $\pm 0.50$ ,  $-6.25$ ,  $-2.25$ ; 1  $\mu$ L) and ( $\pm 0.50$ ,  $-7.20$ ,  $-3.00$ ; 1  $\mu$ L). Three weeks later, mouse brains were removed, sectioned at 100  $\mu$ m thickness, and floated in PBS. Sections were stained with DAPI for 15 min and imaged using confocal microscopy (FV3000, Olympus, Japan).

For mitochondria-targeted labeling experiments, AAV sequences were RAAV-ef1 $\alpha$ -DIO-Mito-mCherry (BC-1577, Braincase, China) and RAAV-ef1 $\alpha$ -DIO-Mito-EGFP (BC-1577, Braincase, China). The injection sites were: ( $\pm 0.50$ ,  $-6.25$ ,  $-2.25$ ; 1  $\mu$ L) and ( $\pm 0.50$ ,  $-7.20$ ,  $-3.00$ ; 1  $\mu$ L). AAV was injected at a rate of 150 nL/min.

### Mitochondria transplantation

After incubation in RIPA on ice for 10 min, mitochondrial proteins concentration was measured by Nanodrop (701-058112, Thermo Scientific, USA). And the mitochondria were diluted to 50 mg/mL. The mice were anesthetized with pentobarbital. Mitochondria (40  $\mu$ g) were injected into cerebellum at sites ( $\pm 0.50$ ,  $-6.25$ ,  $-2.25$ ; 200 nL) and ( $\pm 0.50$ ,  $-7.20$ ,  $-3.00$ ; 200 nL), using a microsyringe (RWD 79013, Shenzhen, China) at speed of 100 nL/min. The needle remained in cerebellum for 8 min before removal. Control mice received an equal volume of storage buffer. The entire procedure was finished within 1 h.

To test mitochondrial bioactivity, mitochondria were stained with Mitotracker Red (100 nM, M22426, Invitrogen, USA) at 37 °C for 30 min, then observed under confocal microscope (FV3000, Olympus, Japan). Additionally, liver-isolated mitochondria stained with Mitotracker green (100 nM, M7514, Invitrogen, USA) were subsequently transplanted into the cerebellum of CBND<sup>general</sup> mice to investigate exogenous mitochondrial persistence.

### CUBIC tissue clearing

The tissue clearing protocol followed the hydrophilic tissue clearing reagent kit (#210701, Nuohai Life Science, China). Mice were perfused with PBS, fixed with 4% paraformaldehyde, and post-fixed with 4% paraformaldehyde again at 4 °C for 24 h. Wash twice with PBS for 2 h. The brain was then immersed in the delipidated solution (solution A:solution B = 1:1) at 37 °C for 6 days with shaking at 60 rpm. Next, the brain was immersed in solution C at 25 °C for refractive index matching with shaking at 60 rpm for 2 days. Finally, the brain was immobilized with AGAR gel and photographed with Nuohai LS 18 Tiling Light Sheet Microscope (Nuohai Life Science, China).

The raw data for 3D image analysis was captured by LiTScan v3.3.0 (Light Innovation Technology Limited) and subsequently converted into Amira-readable format (Version 2023.1, Thermo Fisher Scientific, USA). Subsampling of the 3D image samples was conducted to adjust resolution, utilizing the Resample module to set appropriate voxel sizes. Background noise was eliminated with the background detection



and correction filters, and structural features were enhanced using 3D filters, followed by segmentation of regions of interest using the Interactive Thresholding module. Subsequently, manual labeling of segmented regions was performed, followed by removal of small spots to eliminate defects. PCs and cerebellar regions were treated independently, with cerebellar segmentation accomplished through manual labeling based on atlases. Measurement and analysis modules, especially the label analysis function, were employed for data quantification, with the selection of spreadsheet and spatial map options for result export. Finally, selected data was imported into Imaris software (Version 10.2.0, Oxford Instruments, UK) for visualization representation.

### Mitochondrial network analysis (MiNA) analysis

RAAV-ef1 $\alpha$ -DIO-Mito-EGFP (BC-1577, Braincase, China) was injected to cerebellum. These mice were sacrificed 3 weeks post-injection. The cerebellum was photoed under confocal microscope (Leica stellaris 5). ImageJ (Version 1.54f) was used for MiNA analysis.

### Real time-quantitative polymerase chain reaction (RT-qPCR)

Trizol reagent (DP419, TIANGEN, China) was used to extract the total RNA. Total RNA was reversely transcribed to cDNA using cDNA synthesis kit (TSK314S, TSINGKE, China). The cDNA was used to perform PCR test (TSE201, TSINGKE, China), including Drp1, ATXN1, ATXN6, ATXN7 and ATXN17. GAPDH was used as the reference gene. All these primer sequences were exhibited in the Supplementary Data 3. The PCR protocol included pre-denaturation at 95 °C for 1 min, followed by 40 cycles of denaturation at 95 °C for 10 s, annealing at 60 °C for 10 s, and finally extended at 72 °C for 10 s. The reaction phase was repeated for 40 cycles. DNA products were detected using lysis curves. The quantitative was statistically calculated using the  $2^{-\Delta\Delta Ct}$ .

### Western Blotting

Protein concentration was detected using BCA assay (E-BC-K318-M, Elabscience, China). Samples were electrophoresed on 7.5% or 12.5% SDS-polyacrylamide gels (PG111 and PG113, Epizyme, China) and transferred to a PVDF membrane (IPVH00010, Millipore, USA). The primary antibodies were incubated at 4 °C over 16 h. The details were shown in Supplementary Data 4. The secondary antibodies were incubated at room temperature for 2 h. Bands were visualized using ECL kit (SQ201, EpiZyme, China) and FUSION FX.EDGE (Vilber, French). The results were quantified by Image J software (Version 1.54f).

### Electronic microscope

Mitochondrial pellets were incubated in fixative containing 2.5% glutaraldehyde and 10 nM phosphate buffer for 30 min at room temperature (Servicebio, G1102-100ML). They were washed 3 times with 0.1 M phosphate buffer (pH 7.2) and fixed in 1% osmic acid at 4 °C for 2 h. Next, mitochondria were gradient dehydrated in ethanol, penetrated in Epon-Araldite resin, and polymerized in molds. Semi-thin section was used for positioning, followed by ultrathin sectioning for microstructure analysis. The sections were counterstained with 3% uranyl acetate and 2.7% lead citrate. Finally, mitochondria were observed by JEM1400 transmission electron microscope. Mitochondria sizes were quantified by Image J software (Version 1.54f) and analyzed using PyCharm 2024.2.

### Drug treatment

For the Mdivi-1 experiment<sup>53</sup>, Mdivi-1 (50 mg/kg) was dissolved in 0.1% DMSO and intraperitoneally injected into C57BL/6J mice. The mice were sacrificed 72 h post-treatment. For the FCCP experiment<sup>54</sup>, FCCP (50  $\mu$ M) was dissolved in 0.1% DMSO and intraperitoneally injected

into C57BL/6J mice (10  $\mu$ L/g). The mice were sacrificed 6 h post-treatment. And their livers were extracted to isolate mitochondria.

### Videos recording

In the balance beam experiment, mice were recorded walking from start to finish using a Xiaomi 13. The movement of 1-year-old mice was recorded using a Xiaomi 13. Videos of all CUBIC experimental results were generated by Aivia software (Version 12.1.0, Leica, Germany).

### Statistics and reproducibility

The experiments were randomized. No statistical method was used to predetermine sample size. No data was excluded from the analyses. The investigators were blinded to the intervention methods for the mice. Data was shown as mean  $\pm$  SD. The specific “*n*” values for each experiment are provided in the figure legends. All data was first analyzed for the Normality test and Homogeneity of variance test. One-way ANOVA followed by Dunnett’s *t* test was used for three or more samples comparison. And for two samples comparison, Unpaired two-tailed student’s *t* test was used. Non-parametric data were analyzed using Kruskal-Wallis tests or Mann-Whitney *U* tests. For repeated measurements, two-way ANOVA test and Sidak test were used. Statistical analyses were performed using GraphPad Prism 8.0.2. *P* < 0.05 was considered statistically significant.

### Reporting summary

Further information on research design is available in the Nature Portfolio Reporting Summary linked to this article.

### Data availability

The Source data generated in this study are provided in the Source Data file. Source data are provided with this paper.

### References

1. Takahashi, T. et al. LINE-1 activation in the cerebellum drives ataxia. *Neuron* **110**, 3278–3287.e3278 (2022).
2. Switonski, P. M. et al. Altered H3 histone acetylation impairs high-fidelity DNA repair to promote cerebellar degeneration in spinocerebellar ataxia type 7. *Cell Rep.* **37**, 110062 (2021).
3. Spinocerebellar ataxia. *Nat. Rev. Dis. Primers* **5**, 25 (2019).
4. Beaudin, M., Manto, M., Schmähmann, J. D., Pandolfo, M. & Dupre, N. Recessive cerebellar and afferent ataxias—clinical challenges and future directions. *Nat. Rev. Neurol.* **18**, 257–272 (2022).
5. Monzio Compagnoni, G. et al. The role of mitochondria in neurodegenerative diseases: the lesson from Alzheimer’s disease and Parkinson’s disease. *Mol. Neurobiol.* **57**, 2959–2980 (2020).
6. Baden, P. et al. Glucocerebrosidase is imported into mitochondria and preserves complex I integrity and energy metabolism. *Nat. Commun.* **14**, 1930 (2023).
7. Quinn, P. M. J., Moreira, P. I., Ambrósio, A. F. & Alves, C. H. PINK1/PARKIN signalling in neurodegeneration and neuroinflammation. *Acta Neuropathol. Commun.* **8**, 189 (2020).
8. Zhang, H. et al. SNX14 deficiency-induced defective axonal mitochondrial transport in Purkinje cells underlies cerebellar ataxia and can be reversed by valproate. *Natl. Sci. Rev.* **8**, nwab024 (2021).
9. Chen, H., McCaffery, J. M. & Chan, D. C. Mitochondrial fusion protects against neurodegeneration in the cerebellum. *Cell* **130**, 548–562 (2007).
10. Akhlaghasand, M. et al. Grafted human chorionic stem cells restore motor function and preclude cerebellar neurodegeneration in rat model of cerebellar ataxia. *Metab. Brain Dis.* **35**, 615–625 (2020).
11. Zong, Y. et al. Mitochondrial dysfunction: mechanisms and advances in therapy. *Signal Transduct. Target. Ther.* **9**, 124 (2024).
12. Malpartida, A. B., Williamson, M., Narendra, D. P., Wade-Martins, R. & Ryan, B. J. Mitochondrial dysfunction and mitophagy in parkinson’s

- disease: from mechanism to therapy. *Trends Biochem Sci.* **46**, 329–343 (2021).
13. Johri, A. Disentangling mitochondria in Alzheimer's disease. *Int. J. Mol. Sci.* **22**, 11520 (2021).
  14. Shin, B., Cowan, D. B., Emani, S. M., Del Nido, P. J. & McCully, J. D. Mitochondrial transplantation in myocardial ischemia and reperfusion injury. *Adv. Exp. Med. Biol.* **982**, 595–619 (2017).
  15. Emani, S. M., Piekarski, B. L., Harrild, D., Del Nido, P. J. & McCully, J. D. Autologous mitochondrial transplantation for dysfunction after ischemia-reperfusion injury. *J. Thorac. Cardiovasc. Surg.* **154**, 286–289 (2017).
  16. Jain, R. et al. Inter and intracellular mitochondrial transfer: future of mitochondrial transplant therapy in Parkinson's disease. *Biomed. Pharmacother.* **159**, 114268 (2023).
  17. Huang, P. J. et al. Transferring xenogenic mitochondria provides neural protection against ischemic stress in ischemic rat brains. *Cell Transpl.* **25**, 913–927 (2016).
  18. Chang, J. C. et al. Allogeneic/xenogeneic transplantation of peptide-labeled mitochondria in Parkinson's disease: restoration of mitochondria functions and attenuation of 6-hydroxydopamine-induced neurotoxicity. *Transl. Res.* **170**, 40–56.e43 (2016).
  19. Lin, R. Z. et al. Mitochondrial transfer mediates endothelial cell engraftment through mitophagy. *Nature* **629**, 660–668 (2024).
  20. Nakai, R. et al. Mitochondria transfer-based therapies reduce the morbidity and mortality of Leigh syndrome. *Nat. Metab.* **6**, 1886–1896 (2024).
  21. Kageyama, Y. et al. Mitochondrial division ensures the survival of postmitotic neurons by suppressing oxidative damage. *J. Cell Biol.* **197**, 535–551 (2012).
  22. Nakamura, Y., Park, J. H. & Hayakawa, K. Therapeutic use of extracellular mitochondria in CNS injury and disease. *Exp. Neurol.* **324**, 113114 (2020).
  23. Khan, M. M., Paez, H. G., Pitzer, C. R. & Alway, S. E. The therapeutic potential of mitochondria transplantation therapy in neurodegenerative and neurovascular disorders. *Curr. Neuropharmacol.* **21**, 1100–1116 (2023).
  24. Patel, S. P. et al. Delivery of mitoceuticals or respiratory competent mitochondria to sites of neurotrauma. *Mitochondrion* **68**, 10–14 (2023).
  25. Kaza, A. K. et al. Myocardial rescue with autologous mitochondrial transplantation in a porcine model of ischemia/reperfusion. *J. Thorac. Cardiovasc. Surg.* **153**, 934–943 (2017).
  26. Shin, B. et al. A novel biological strategy for myocardial protection by intracoronary delivery of mitochondria: safety and efficacy. *JACC Basic Transl. Sci.* **4**, 871–888 (2019).
  27. Picone, P. & Nuzzo, D. Promising treatment for multiple sclerosis: mitochondrial transplantation. *Int. J. Mol. Sci.* **23**, 2245 (2022).
  28. Alexander, J. F. et al. Nasal administration of mitochondria reverses chemotherapy-induced cognitive deficits. *Theranostics* **11**, 3109–3130 (2021).
  29. Hayakawa, K. et al. Transfer of mitochondria from astrocytes to neurons after stroke. *Nature* **535**, 551–555 (2016).
  30. Berridge, M. V., Schneider, R. T. & McConnell, M. J. Mitochondrial transfer from astrocytes to neurons following ischemic insult: guilt by association? *Cell Metab.* **24**, 376–378 (2016).
  31. Ni, X. C. et al. Ginsenoside Rb1 inhibits astrocyte activation and promotes transfer of astrocytic mitochondria to neurons against ischemic stroke. *Redox Biol.* **54**, 102363 (2022).
  32. Scheiblich, H. et al. Microglia rescue neurons from aggregate-induced neuronal dysfunction and death through tunneling nanotubes. *Neuron* **112**, 3106–3125.e3108 (2024).
  33. Kraus, F., Roy, K., Pucadyil, T. J. & Ryan, M. T. Function and regulation of the divisome for mitochondrial fission. *Nature* **590**, 57–66 (2021).
  34. Jiao, H. et al. Mitocytosis, a migrasome-mediated mitochondrial quality-control process. *Cell* **184**, 2896–2910.e2813 (2021).
  35. Kleele, T. et al. Distinct fission signatures predict mitochondrial degradation or biogenesis. *Nature* **593**, 435–439 (2021).
  36. Fan, R. Z. et al. A partial Drp1 knockout improves autophagy flux independent of mitochondrial function. *Mol. Neurodegener.* **19**, 26 (2024).
  37. Wong, Y. C. & Holzbaur, E. L. Optineurin is an autophagy receptor for damaged mitochondria in parkin-mediated mitophagy that is disrupted by an ALS-linked mutation. *Proc. Natl. Acad. Sci. USA* **111**, E4439–E4448 (2014).
  38. Narendra, D. P. & Youle, R. J. The role of PINK1-Parkin in mitochondrial quality control. *Nat. Cell Biol.* **26**, 1639–1651 (2024).
  39. Lu, Y. et al. Cellular mitophagy: mechanism, roles in diseases and small molecule pharmacological regulation. *Theranostics* **13**, 736–766 (2023).
  40. Lou, G. et al. Mitophagy and neuroprotection. *Trends Mol. Med.* **26**, 8–20 (2020).
  41. Kerr, J. S. et al. Mitophagy and Alzheimer's disease: cellular and molecular mechanisms. *Trends Neurosci.* **40**, 151–166 (2017).
  42. Li, M. et al. DDIT3 directs a dual mechanism to balance glycolysis and oxidative phosphorylation during glutamine deprivation. *Adv. Sci.* **8**, e2003732 (2021).
  43. Cheng, X. et al. Overexpression of Kininogen-1 aggravates oxidative stress and mitochondrial dysfunction in DOX-induced cardiotoxicity. *Biochem. Biophys. Res. Commun.* **550**, 142–150 (2021).
  44. Liu, H. et al. New insights into brain injury in chickens induced by bisphenol A and selenium deficiency-Mitochondrial reactive oxygen species and mitophagy-apoptosis crosstalk homeostasis. *Sci. Total Environ.* **905**, 166890 (2023).
  45. Nicolás-Ávila, J. A. et al. A network of macrophages supports mitochondrial homeostasis in the heart. *Cell* **183**, 94–109.e123 (2020).
  46. Sudhakar, V. & Richardson, R. M. Gene therapy for neurodegenerative diseases. *Neurotherapeutics* **16**, 166–175 (2019).
  47. Mendell, J. R. et al. Current clinical applications of in vivo gene therapy with AAVs. *Mol. Ther.* **29**, 464–488 (2021).
  48. Rafii, M. S. et al. A phase1 study of stereotactic gene delivery of AAV2-NGF for Alzheimer's disease. *Alzheimers Dement.* **10**, 571–581 (2014).
  49. Rafii, M. S. et al. Adeno-associated viral vector (serotype 2)-nerve growth factor for patients with Alzheimer disease: a randomized clinical trial. *JAMA Neurol.* **75**, 834–841 (2018).
  50. Al-Zaidy, S. et al. Health outcomes in spinal muscular atrophy type 1 following AVXS-101 gene replacement therapy. *Pediatr. Pulmonol.* **54**, 179–185 (2019).
  51. Gordon, R. et al. Inflammasome inhibition prevents  $\alpha$ -synuclein pathology and dopaminergic neurodegeneration in mice. *Sci. Transl. Med.* **10**, eaah4066 (2018).
  52. Rana, A. et al. Pantethine rescues a Drosophila model for pan-tothenate kinase-associated neurodegeneration. *Proc. Natl. Acad. Sci. USA* **107**, 6988–6993 (2010).
  53. Yang, Y. et al. Bavachin induces liver injury and cell apoptosis by targeting Wnt/ $\beta$ -catenin/DRP1 signaling pathway mediated mitochondrial dysfunction. *Toxicol. Lett.* **387**, 1–13 (2023).
  54. Wang, Y. T. et al. Cardioprotection by the mitochondrial unfolded protein response requires ATF5. *Am. J. Physiol. Heart Circ. Physiol.* **317**, H472–H478 (2019).

## Acknowledgements

We thank all members of Y.Y.W.'s lab for their insightful and helpful discussions during the course of the study. This project was supported by the Military Medicine Upgrade Program of Air Force Military Medical University (2020SWAQ04) from Y.Y.W., the Shaanxi Innovation Capability Support Plan (2023-CX-PT-33) from Y.Y.W., the Shaanxi Basic

Research Program of Natural Sciences (2024JC-ZDXM-60) from Y.L.Y., the Xi-Jing Hospital Clinical New technology (2023XJSY27) from Y.L.Y., the Shaanxi Basic Research Program of Natural Science (2022JQ-820) from F.F.W., and the National Natural Science Foundation of China (82201627) from F.F.W.

## Author contributions

Y.Y.W., Y.L.Y., and X.S. conceptualized the project. Y.Y.W. and S.J.L. designed experiments and wrote the manuscript. S.J.L. carried out behavior tests, mitochondria transplantation experiments, and virus regulation experiment. Q.W.Z. and J.Z. conducted behavior tests, Western blot experiments and data analysis, mice genotype test and draw the cartoon images. J.B.Z. analyzed the data. H.L. performed the RNA-scope experiments. J.J.T. performed RT-PCR experiments. K.L.Z. and F.F.W. conducted virus regulation experiment. X.D.L. and S.Z. performed images analysis. All of the authors read and approved the final manuscript.

## Competing interests

The authors declare no competing interests.

## Additional information

**Supplementary information** The online version contains supplementary material available at <https://doi.org/10.1038/s41467-025-58189-4>.

**Correspondence** and requests for materials should be addressed to Xin Sun, Yan-Ling Yang or Ya-Yun Wang.

**Peer review information** *Nature Communications* thanks Jonathan Brestoff, Alanna Watt, and the other, anonymous, reviewer for their contribution to the peer review of this work. A peer review file is available.

**Reprints and permissions information** is available at <http://www.nature.com/reprints>

**Publisher's note** Springer Nature remains neutral with regard to jurisdictional claims in published maps and institutional affiliations.

**Open Access** This article is licensed under a Creative Commons Attribution-NonCommercial-NoDerivatives 4.0 International License, which permits any non-commercial use, sharing, distribution and reproduction in any medium or format, as long as you give appropriate credit to the original author(s) and the source, provide a link to the Creative Commons licence, and indicate if you modified the licensed material. You do not have permission under this licence to share adapted material derived from this article or parts of it. The images or other third party material in this article are included in the article's Creative Commons licence, unless indicated otherwise in a credit line to the material. If material is not included in the article's Creative Commons licence and your intended use is not permitted by statutory regulation or exceeds the permitted use, you will need to obtain permission directly from the copyright holder. To view a copy of this licence, visit <http://creativecommons.org/licenses/by-nc-nd/4.0/>.

© The Author(s) 2025